Epitranscriptomic landscape of vascular smooth muscle cell phenotypic transitions highlights uridine RNA modifications associated with post-transcriptional regulation

Tobias Reinberger[1,2], Ayat Ismail[3], Torben Falk[1,2], Janina Fuß[4], Anja Wiechert[5,6], Elke Hammer[5,6], Tanja Zeller[1,2], Inken Wohlers[3,7,8,9*]

[1] Institute for Cardiogenetics, University Heart Center Lübeck, University Medical Center Schleswig-Holstein, Universität zu Lübeck, Germany

[2] DZHK (German Centre for Cardiovascular Research), Partner Site Hamburg/Kiel/Lübeck, Germany; University Heart Centre Lübeck, 23562 Lübeck, Germany

[3] Biomolecular Data Science in Pneumology, Research Center Borstel, Leibniz Lung Center, Borstel, Germany

[4] Institute of Clinical Molecular Biology, Christian-Albrechts-University of Kiel, Kiel, Germany

[5] Department Functional Genomics, Interfaculty Institute of Genetics and Functional Genomics, University Medicine Greifswald, Greifswald, Germany

[6] DZHK (German Center for Cardiovascular Research), Greifswald, Germany

[7] University of Lübeck, Lübeck, Germany

[8] College of Medicine & Health Sciences, Khalifa University for Science and Technology, Abu Dhabi, United Arab Emirates

[9] Airway Research Center North (ARCN), German Center for Lung Research (DZL), Borstel, Germany

*Correspondence to iwohlers@fz-borstel.de, Research Center Borstel, Leibniz Lung Center, Parkallee 1, 23845 Borstel, Germany

Abstract

Background

Vascular smooth muscle cells (VSMCs) reside in the medial arterial wall and are involved in the regulation of vascular tone and remodeling. VSMCs possess phenotypic plasticity, contributing to subclinical atherosclerosis. The processes of VSMC phenotypic transitions from the contractile to pro-inflammatory phenotypes are well-studied. However, epitranscriptomic changes during this transition and their regulatory role remain unexplored.

Methods

Primary human VSMCs were stimulated with TGF-β1 to induce an atheroprotective, contractile state and with IL1-β plus PDGF-BB to induce a pro-inflammatory state. Sequentially treated VSMCs were further stimulated with PDGF-BB to induce oxidative stress. Transcriptome profiling was performed using Illumina bulk RNA sequencing and epitranscriptomic profiling using Oxford Nanopore Technologies direct RNA sequencing. Potential post-transcriptional regulatory effects of RNA modifications were assessed using small RNA sequencing and proteomics.

Results

Transcriptomic changes globally reflected atheroprotective and pro-atherogenic treatments, with oxidative stress inducing the largest gene expression changes. Significant differential RNA modifications were detected mainly between atheroprotective and pro-atherogenic VSMCs. Differences in modification predominantly affected uridine within a GUUUU motif, enriched in 3'-UTR and accessible RNA structures. Poly(A) tail lengths of modified transcripts differed between conditions, and transcripts with more modifications showed increased translation efficiency. Highly expressed microRNAs (miRNAs) had predicted binding sites overlapping about 5% of differential modification sites.

Conclusions

Atheroprotective and pro-atherogenic treatments induce distinct epitranscriptomic landscapes composed of different modification types in diverse sequence contexts, often co-localized in the same transcript. Differences in poly(A) tail lengths and translation efficiency for genes with different RNA modifications suggest that modifications play a post-transcriptional regulatory role. Uridine modifications were most abundant, enriched in 3'-UTRs and accessible structures, hinting at miRNA-based regulation. Many highly expressed miRNAs may have binding affected by RNA modifications. In summary, epitranscriptomics adds a novel regulatory layer to VSMC phenotypic transitions with implications for atherosclerosis development and progression.

Keywords: Epitranscriptomics, RNA Modifications, Vascular Smooth Muscle Cells, Phenotypic Transition, Post-Transcriptional Regulation

Novelty and Significance

What is Known?

- VSMC phenotypic switches play a role in the pathogenesis of atherosclerosis, affecting plaque development
- PDGF-BB and IL-1β are important cytokines in the progression of atherosclerosis, inducing VSMC transitions
- Inflammatory diseases and vascular remodeling are associated with RNA base modifications

What New Information Does This Article Contribute?

- Transcriptome-wide characterization of RNA modifications in vascular smooth muscle cell phenotypic transitions, a major hallmark of atherosclerosis, shows that

transcripts are often affected by multiple modifications affecting different bases, adding a level of regulatory complexity that is currently only accessible by direct RNA sequencing methods.

- Differential uridine modifications between TGF-β1-treated VSMCs, representing a healthy, contractile phenotype, and combined PDGF-BB / interleukin-1β-treated VSMCs, representing a pro-inflammatory state, were most common and enriched in the 3'-UTR and in accessible RNA structure elements, indicating epitranscriptomic regulatory effects.
- RNA modifications were located in binding sites of many highly expressed miRNAs, and modified transcripts showed significant differences in poly(A) tail length as well as altered translation dynamics, indicating that epitranscriptomics plays a role in post-transcriptional regulation.

We characterized VSMC phenotypic transitions from Illumina short-read sequencing data and – for the first time – corresponding RNA modifications from Oxford Nanopore Technologies (ONT) direct RNA long-read sequencing. We found that oxidative stress results in the largest difference in expression between conditions. On the contrary, no major modification differences were detectable under oxidative stress. The largest numbers of differentially modified sites were observed between the healthy, contractile phenotype and the synthetic phenotypes, with the most abundant modified base being uridine. While differences in pseudouridine synthases between contractile and oxidative stress conditions indicate pseudouridylation, further mechanisms seem to play a role. Towards this, we investigated differences in microRNA (miRNA) binding as a possible mechanism underlying differentially modified sites and identified miRNAs that were previously described to play a role in VSMC phenotypic transition and cardiovascular disease. Thus, this first characterization of RNA modifications in VSMC phenotypic transitions suggests uridine

modifications as a major factor and hints towards miRNA binding as a modulator of RNA modifications.

Introduction

Vascular cell adaptation within atherosclerotic plaques is one of the key features that modulate disease progression and can define the severity of atherosclerotic outcomes.[1] In particular, the immense plasticity of vascular smooth muscle cells (VSMCs) has been one of the research focuses in cardiovascular disease over the last years. While cytokine-driven pathways, key transcription factors, epigenetic mechanisms, and non-coding RNAs are well described to shape VSMC phenotypic transitions[2–5], the influence of epitranscriptomic regulation remains largely unexplored and is only beginning to receive attention. [6]

Epitranscriptomics characterizes and quantifies the collective set of chemical modifications of RNA. Previously, such modifications were investigated with techniques only dedicated to specific modification types, such as N6-methyladenosine (m^6A) and RNA types such as rRNA or tRNA.[7] With technological developments in third-generation sequencing, epitranscriptome-wide investigations are becoming feasible. Thereby, direct RNA sequencing of Oxford Nanopore Technologies (ONT) allows the hypothesis-free identification of modification sites by determining significant electric current differences between modified and unmodified bases, measured while RNA passes through a nanopore.[8] More than 100 different types of RNA modifications have been described, and associations with many diseases have been reported.[9] Technology-fueled increased interest resulted in a few initial enzyme or modification-centered investigations in vascular disease published within the past five years.[10,11] The importance of epitranscriptomic regulation in VSMC phenotypic transitions is in the early stages of being recognized. For example, platelet-derived growth factor (PDGF)-BB-induced adenosines to inosines (A-to-I) editing has been described to foster the transition from the contractile, quiescent to a synthetic, pro-inflammatory VSMC state.[12] In contrast, it has been demonstrated that m^6A mRNA

methylation stabilizes transcripts of genes involved in VSMC-mediated vasoconstriction, thereby highlighting the clinically relevant role of epitranscriptomic control in blood pressure.[13] Another disease-relevant RNA modification is 8-oxo-guanosine (8-oxoGuo), a product of RNA oxidation, which has been associated with atherosclerosis and reported as a predictor of mortality in individuals with type 2 diabetes.[14] Although the molecular consequences of RNA guanosine oxidation are well described in the context of cardiovascular diseases[15], the direct implication in VSMC biology remains elusive. Nevertheless, oxidative stress is widely accepted to play a key role in chronic inflammation, to contribute to VSMC phenotypic switching[16], and to promote the development of unstable plaques[17]. Therefore, we used hypothesis-free ONT direct RNA sequencing to entangle the global epitransctriptomic landscape of various VSMC phenotype states.

Inspired by a recent study in which ONT long-read cDNA sequencing has been applied to investigate alternative splicing of contractile and proliferative, pro-inflammatory phenotypes, represented by transforming growth factor β1 (TGF-β1)- and PDGF-BB-treated human aortic smooth muscle cells[18], we treated VSMCs with TGF-β1 to promote an atheroprotective state (later referred to as condition C3). This VSMC phenotype was compared to pro-inflammatory/pro-atherogenic VSMCs under PDGF-BB / interleukin 1β (IL-1β) treatment[19] (condition C4), and additionally to oxidative stress-prone VSMCs (C2) as well as oxidatively stressed VSMCs (C1). Here, we demonstrate that epitranscriptomic alterations drive post-transcriptional regulation by affecting mRNA processing, miRNA binding, and translation, thereby determining VSMC states important for atherosclerotic disease progression.

Methods

Cell culture of vascular smooth muscle cells

In total, eight human primary VSMC lines were purchased from several vendors. VSMCs were cultured in M231 cell culture medium (Gibco M-213-500) with 1x Smooth Muscle

161 Growth Supplement (SMGS) (Gibco S-007-25) at 37 °C and 5% carbon dioxide (CO2) in
162 T75 or T175 flasks (Greiner). VSMCs were split at a maximum of 80% confluency until a
163 maximum of eight passages. VSMCs were washed with 1x phosphate-buffered saline (PBS)
164 before detachment with 1x trypsin/EDTA for up to 5 min at 37 °C. VSMCs were seeded on a
165 collagen I hydrogel (Ibidi, 5 mg/mL, collagen type I, rat tail) for CellROX assays, Nanopore
166 RNA sequencing, and Illumina RNA sequencing (see below). In brief, collagen I (Col I) was
167 thawed at 4 °C at least two hours before use. A solution of 300 µL Col I hydrogel (1.5
168 mg/mL) was prepared by mixing the following components (stored at 4 °C) in the exact order
169 on ice: 20 µL of 10x SMGS, 5 µL of 1 M NaOH (Roth K021.1), 81 µL ddH_2O
170 (Double-distilled, invitrogen 10977-035), 4 µL of $NaHCO_3$ (7.5%, w/v, Biochemka 71627),
171 100 µL M321 cell culture medium, and 90 µL of 5 mg/mL Col I. Pour slowly into a tube and
172 mix carefully by pipetting up and down. The solution should have a pH of 6.5 - 7.5 (optimally
173 7.0). The freshly prepared Col I hydrogel was pipetted into each well/flask on ice. To enable
174 polymerization, Col I hydrogel plates were stored at 37 °C for 30-60 min. In total, 0.2 mL and
175 1.8 mL of Col I hydrogel were used per well of a 48-well plate and a 6-well plate,
176 respectively. After polymerization, 0.4×10^5 cells/well and 3.8×10^5 cells/well were seeded in a
177 48-well plate and a 6-well plate, respectively, and were incubated for 24 hours in M321 cell
178 culture medium supplemented with 1% fetal bovine serum (FBS, BioSell FBS.GP.0500). In
179 addition, 1 µM cytochalasin D (Sigma C2618) was added to inhibit VSMC contraction.[20] To
180 induce the contractile phenotype of VSMCs, cells were incubated in fresh M321 medium
181 supplemented with 1% FBS, 5 ng/mL human recombinant TGF-β1 (Transforming Growth
182 Factor Beta 1, Peprotech 100-21C), and 1 µM cytochalasin D for four days. The transition
183 from the contractile VSMC phenotype to a synthetic VSMC phenotype was achieved by
184 replacing the old medium with fresh M321 medium (without cytochalasin D) supplemented
185 with 1% FBS, 10 ng/mL human recombinant PDGF-BB (Platelet-Derived Growth Factor),
186 and 10 ng/mL human recombinant IL-1β (Interleukin-1β). VSMCs were cultured for two days
187 under these pro-inflammatory conditions.

188

189 *Oxidative stress assays in vascular smooth muscle cells*

190 Two male human aortic VSMC lines and four technical replicates per VSMC line were used
191 for oxidative stress assays: HAOSMC IV (Thermo Fisher Scientific, C-007-5C, LOT:
192 2164581) and HAOSMC 1596 (Cell Applications, Inc., 354-05a, LOT: 354-05a). To check for
193 sex differences, two female human VSMC lines were also analyzed: HAOSMC III (Cell
194 Applications, Inc., 354-05a, LOT: 2228) and HAOSMC VIII (Promocell, C-12533, LOT:
195 431Z013.6). VSMCs were seeded on a Col I hydrogel and incubated in M231 cell culture
196 medium supplemented as described above in detail: 1) one day in M231 + 1% FBS, 2) four
197 days with or without 5 ng/mL TGF-β1, and 3) two days with or without 10 ng/mL PDGF-BB
198 and 10 ng/mL IL-1β. To induce measurable endogenous production of reactive oxygen
199 species (ROS), VSMCs were treated with 200 ng/mL PDGF-BB for 1 – 2 hours (referred to
200 as PDGF boost), 30 µM CellROX® Green reagent (Invitrogen™, C10444), and 1 µg/mL
201 Hoechst 33342 (Merck #14533-100MG) in M231 + 1% FBS. To further boost production of
202 reactive oxygen species (ROS), VSMCs were exposed to ultraviolet (UV) radiation for 5
203 minutes. VSMCs without PDGF boost but with CellROX® Green reagent served as a
204 negative control. N-Acetylcysteine (NAC), a potent antioxidant[21], served as the second
205 control and was added two hours prior to and during the CellRox assay at a total
206 concentration of 1 mM to quench ROS production. CellROX® Green fluorescent levels were
207 measured with an immunofluorescence microscope (Keyence BZ-X800) using 10 µm
208 z-stacks at 10-fold magnification and quantified with an in-house Python script. CellROX®
209 Green fluorescent levels were normalized against Hoechst 33342 staining of nuclei.

210

211 *Quantification of the mitochondrial membrane potential*

212 The VSMC line HAOSMC IV was used to quantify the mitochondrial membrane potential
213 (MMP) and the number of mitochondria (numMT) under different stimuli. Approximately
214 0.4×10^5 cells/well were seeded in 96-well plates (for MMP) or 8-well Lab Tek chamber slides

215 (for numMT) previously coated with 1% porcine gelatine. After one day of incubation in
216 M231 cell culture medium with SMGS, the medium was replaced with fresh M231 cell
217 culture medium with 1% FBS. Cells were stimulated like the CellROX® assays as described
218 above. To measure the MMP, cells were incubated with 200 nM TMRE
219 (tetramethylrhodamine ethyl ester perchlorate, Invitrogen™ T669) in M231 + 1% FBS for 30
220 minutes at 37 °C and 5% CO2, washed with PBS, incubated with 1 µg/mL Hoechst 33342
221 for 20 minutes, washed twice with PBS, and fixated with cold 4% paraformaldehyde (PFA)
222 for 20 minutes. To quench the MMP completely, 10 µM FCCP (Carbonyl
223 cyanide-p-trifluoromethoxyphenylhydrazone; Sigma), a proton uncoupling agent, was added
224 as a negative control. To check for the number of mitochondria (numMT), stimulated cells
225 (see above) were fixated with cold 4% PFA for 10 minutes and stored at -20 °C until usage.
226 On the day of staining, frozen cells on chamber slides were directly fixated in
227 acetone-methanol (stored at -20°C) for 10 minutes. Cells were permeabilized with 0.1%
228 Triton X-100 (Sigma 23.472-9) + 1% bovine serum albumin (BSA) for 30 minutes at room
229 temperature (RT). Cells were blocked with 3% BSA in PBS for 1 hour at RT. Finally, cells
230 were stained with an anti-GRP75 antibody (abcam ab53098, 1:1000) and an anti-β-Actin
231 antibody (Sigma A5228, 1:500). Primary antibodies were visualized with Alexa Fluor 488
232 (Thermo Fisher Scientific, A11011) or Alexa Fluor 568 antibodies 488 (Thermo Fisher
233 Scientific, A10037; 1:1000 dilution). TRME, GRP75, and Hoechst 33342 were quantified as
234 described above (see CellROX® assays) using an immunofluorescence microscope
235 (Keyence BZ-X800) and a Python script.

236

237 *Seahorse assays for vascular smooth muscle cell respiration*

238 The VSMC line HAOSMC IV was used for Seahorse assays. Approximately 0.4×10^5
239 cells/well were seeded in 24-well cell culture plates (Agilent #100777-004), leaving 4 wells
240 blank. Cells were stimulated like the CellROX® assays as described above. Incubation with
241 200 ng/mL PDGF-BB was extended to 4 hours. Untreated cells served as the control. Five

242 wells per condition were used as technical replicates. Seahorse experiments were repeated
243 five times. XF24 sensor cartridges (Agilent #100850-001) were incubated overnight in
244 Agilent calibrant solution at 37 °C under an ambient atmosphere. Approximately 1 hour
245 before measurement, the cell culture medium was replaced by Seahorse XF DMEM assay
246 (Agilent #103681-100) supplemented with 1 mM Pyruvate (Gibco), 4 mM L-glutamate
247 (Gibco), and 10 mM Glucose (Sigma). To measure changes in oxygen consumption rate
248 (OCR) and extracellular acidification rate (ECAR) using a Seahorse XF24 analyzer, 1.4 µM
249 oligomycin (Sigma), 1 µM FCCP (Sigma), and 1.5 µM antimycin A/1.5 µM rotenone were
250 added sequentially in each well. Each OCR measurement consisted of 1 min of mixing, 2
251 min of waiting, and 4 min of continuous O_2 level measurement. Cells were stained with
252 Hoechst 33342 (Merck #14533-100MG) and counted to normalize OCRs. All Seahorse
253 parameters (*e.g.*, basal respiration or ATP production) were calculated according to the
254 manufacturer's instructions.
255
256 *Short-read RNA sequencing*
257 Short-read sequencing (NovaSeq6000, 2x100 bp) using the TrueSeq stranded mRNA library
258 preparation kit without polyA enrichment was performed for eight biological replicates (see
259 **Suppl. Table S1**) and five conditions (oxidative-stressed VSMCs (C1), oxidative
260 stress-prone VSMCs (C2), atheroprotective VSMCs (C3), proatherogenic VSMCs (C4), and
261 untreated VSMCs (C5)). Stimulation of VSMCs was conducted similarly to the CellROX®
262 assays. Approximately 3.8×10^5 cells/well were seeded in 6-well plates that were covered
263 with a Col I hydrogel (1.8 mL with 1.5 mg/mL). At least two wells per condition were
264 prepared, and VMCS were harvested by incubating with 0.1% (w/v) collagenase type 2 in
265 PBS (Cellsystems LS004176) for 15 minutes at 37 °C. Detached cells were centrifuged at
266 300×g for 5 minutes. The cell pellets were frozen at -80 °C until further usage. Total RNA (5
267 µg per reaction) was isolated using the innuPREP RNA Mini Kit 2.0 (Analytik Jena)
268 according to the manufacturer's instructions. Depletion of ribosomal RNA (rRNA) was

269 achieved with magnetic beads using the RiboMinus™ Eukaryote System v2 (Invitrogen
270 A15026) according to the manufacturer's instructions. To remove all residues of the
271 hybridization buffer, the magnet beads were washed twice instead of once. The
272 rRNA-depleted RNA was concentrated from 300 µl supernatant with RNA clean XP beads
273 (Beckman Coulter A63987). Initially, 660 µL of XP beads were added to a 1.5 mL tube and
274 placed on a magnetic rack to allow separation. After removing 120 µL supernatant, the
275 beads were resuspended and incubated at 65°C for 2 minutes. The bead suspension was
276 added to the 300 µL RNA sample and mixed gently using a pipette. The mixture was
277 incubated at RT for 15 minutes on a HoLa shaker to facilitate binding. Following this, the
278 tube was placed on a magnetic rack to separate the beads, and the supernatant was
279 removed and discarded. The beads were washed with 70% freshly prepared ethanol by
280 rotating the tube 180° twice, followed by removal of the supernatant. The RNA-loaded beads
281 were air-dried for 2–5 minutes before being resuspended in 30 µL RNase/DNase-free H_2O
282 or RNase/DNase-free TE buffer (Invitrogen 12090015). To elute the RNA, the sample was
283 incubated at 65°C for 1 minute, followed by 4 minutes at RT. Beads were separated using a
284 magnetic rack, and the supernatant containing the purified RNA was transferred to a new
285 tube. RNA concentration was determined with the Qubit RNA HS Assay (Invitrogen Q32852)
286 according to the manufacturer's instructions. The concentration of rRNA-depleted RNA was
287 in a range of 2.7 ng/µL to 5.3 ng/µL.
288
289 *Short-read RNA sequencing data analyses*
290 Five conditions (oxidative stressed VSMCs (C1), oxidative stress-prone VSMCs (C2),
291 atheroprotective VSMCs (C3), proatherogenic VSMCs (C4), and untreated VSMCs (C5))
292 were sampled with eight different VSMC cell lines as biological replicates, generating overall
293 40 RNA sequencing (RNA-Seq) datasets. These were analyzed using a community
294 workflow from the snakemake workflow catalog
295 (https://github.com/snakemake-workflows/rna-seq-kallisto-sleuth) version 2.8.4. This entails

296 expression quantification with kallisto[22] and testing for differential expression using sleuth[23],
297 for which the cell line was considered as a batch variable in the model. For raw and trimmed
298 read QC, FASTQC was used (https://www.bioinformatics.babraham.ac.uk/projects/fastqc),
299 and a combined QC report including mapping statistics was generated using MULTIQC[24].
300 For transcript annotation, Ensemble release 113 was used. Enrichment was computed via
301 the workflow and used SPIA[25] internally for Reactome[26] and KEGG[27] pathways and
302 GOATOOLS[28] for determining enriched Gene Ontology terms. Computation of switches
303 between different isoforms of a gene was also computed via the workflow using the
304 Biocondutor library IsoformSwitchAnalyzeR[29]. Principal component analysis (PCA) was
305 performed for the 1,000 most variable genes after selecting the most highly expressed
306 transcript per gene and keeping only transcripts with a minimum normalized log2 expression
307 of 6.
308
309 *Long-read direct RNA sequencing by Oxford Nanopore Technologies*
310 The VSMC line HAOSMC IV was subjected to direct RNA-Seq using Oxford Nanopore
311 Technologies (ONT) (**Suppl. Table S1**). Four conditions (oxidative stressed VSMCs (C1),
312 oxidative stress-prone VSMCs (C2), atheroprotective VSMCs (C3), proatherogenic VSMCs
313 (C4)) were sequenced. For this, approximately 5×10^5 cells were seeded into one T25 flask
314 covered with 2 mL of 1.8 mg/ml Col I hydrogel. Stimulation, sample preparation, and RNA
315 isolation were performed as described above for short-read RNA-Seq. To trigger
316 endogenous ROS production, VSMCs were incubated with 400 ng/mL PDGF-BB for 3
317 hours. Approximately 10×10^6 stimulated cells per condition were used as input for direct
318 RNA-Seq. Library preparation and direct RNA-Seq were conducted according to the ONT
319 protocol SQK-RNA002 (version DRS_9080_v2_revQ_14Aug2019). About 150 – 200 ng
320 rRNA-depleted RNA in 10 µL was used as input. A GridION device with FLO-MIN106 flow
321 cells with more than 1000 active pores was used for sequencing. Direct RNA-Seq runs were
322 stopped after 18 - 22 hours.

ONT direct RNA sequencing data analyses

ONT direct RNA-Seq data was processed using our own snakemake workflow available at https://github.com/iwohlers/2025_ont_rnaseq_vsmc, with tools installed in a reproducible fashion via conda using environment files provided as part of the workflow. The workflow uses guppy version 6.3.2 for basecalling and pycoQC[30] for quality control. Expression quantification was performed after mapping to hg38 using minimap2[31] with option '-x splice' followed by nanocount[30] with mRNA transcript annotation from Ensembl version 113 (http://ftp.ensembl.org/pub/release-113/gtf/homo_sapiens/Homo_sapiens.GRCh38.113.gtf.gz). Mapping to Ensembl version 13 transcript sequences (http://ftp.ensembl.org/pub/release-113/fasta/homo_sapiens/cdna/Homo_sapiens.GRCh38.cdna.all.fa.gz) was performed with minimap2 using option '-x map-ont'. Primary mappings were used with nanopolish for event preprocessing (mode 'eventalign') and poly(A) tail length estimation (mode 'polya', coverage>10). For differential modification detection, xPore[8] version 2.1 was used with the nanopolish eventalign output, *i.e.*, modification positions refer to transcript coordinates. K-mer transcript positions from xPore (zero-based) were converted to relative genomic positions using pyensembl (https://github.com/openvax/pyensembl) and were converted to relative UTR and coding sequence (CDS) positions using the GFF3 file from Ensembl version 113.

Normalization of nanocount counts and testing of differential expression were performed with DESeq2[32], and an additional variance stabilization using rlog transformation was performed before principal component analysis, both as previously described for nanocount expression data.[30] These downstream analyses and visualizations are available as part of the FAIRDOMHub under https://fairdomhub.org/projects/461.

Transcriptome-wide prediction of RNA structure elements

RNA secondary structures were predicted and plotted with Python 3.11 using the ViennaRNA package library (https://github.com/ViennaRNA/ViennaRNA and https://www.tbi.univie.ac.at/RNA/ViennaRNA/refman/index.html; version 2.6.2) and the Forgi package library (https://github.com/ViennaRNA/forgi). In brief, 150-base mRNA sequences containing the modified base/k-mer were extracted (Ensembl version 113, see above). The first context sequence starts at -140 bases upstream and ends +10 bases downstream of the modified base. The sequence was shifted iteratively by two bases until the start base was -10 bases upstream, yielding up to 65 sequences per transcript and kmer. For each sequence, the centroid structure and corresponding minimum free energy (MFE in kcal/mol) were predicted. The centroid structure refers to a representative secondary structure derived from a Boltzmann-weighted ensemble of possible RNA conformations. The dot-bracket notation of the centroid structure (minus 10 bases at 5’ and 3’ end) was used to calculate the similarity score between all predicted structures using the Needleman-Wunsch algorithm (match score = 1, mismatch penalty = -1, gap penalty = -2). To speed up the algorithm, the similarity score was set to zero if the difference of MFE between the centroid structures was more than 10 kcal/mol. The similarity score was set to one if the centroid structures were the same. Centroid structures were clustered using hierarchical clustering implemented in SciPy. Clusters with the lowest mean MFE, the smallest MFE deviation, and the highest number of centroid structures were considered the best representatives of the RNA secondary structure. The five centroid structures with the lowest MFE of this representative cluster were used for further analysis. The Forgi package was used to convert the dot-bracket notation into secondary structure elements, such as unpaired nucleotides at the 5' end (f), stems or stacked bases (s, regions of contiguous canonical Watson-Crick base-paired nucleotides), hairpin loops (h, single-stranded regions enclosed by a stem), multiloop segments (m, a single-stranded region between two stems), interior loops (i, bulged out regions), and unpaired nucleotides at the 3' end (t). The over-representation

375 analysis of secondary structure elements in kmers was conducted using the hypergeometric
376 distribution function or Fisher's exact test calculated with SciPy.stats in Python. The
377 background was overlapping counts of RNA secondary structure elements across all
378 sequences.
379
380 *Prediction of RNA structure elements with miRNA binding*
381 Wide-window prediction (>350 nt) of RNA secondary structures was conducted with
382 RNAplfold (version 2.7.0) with winsize=150, span=100, and default ulength=31. Alignment of
383 the miRNA to the target sequence was performed by applying first local alignment
384 (Smith-Waterman method without wobble bases; match=1, mismatch_penalty=-2,
385 gap_penalty=-2) of the miRNA seed sequence and the complete transcript sequence,
386 followed by global alignment (Needleman-Wunsch method with allowed wobble bases;
387 match=1, wobble=1, mismatch_penalty=-1.5, gap_penalty=-2) of the complete mature
388 miRNA sequence and the target sequence, which consists of the miRNA binding region
389 extended by a 20 base upstream window. The RNA secondary structure of ITGB1-204,
390 together with miR-493-5p, was plotted as a force-directed graph (Kamada-Kawai layout)
391 with the Python package networkx. Base pairs were created if the base pair probability was
392 above 0.5, and pseudoknots were excluded. Hairpin structures were kept only if at least
393 three consecutive stacked bases were present in the stem region.
394
395 *Small RNA sequencing*
396 For the identification of highly expressed miRNAs, small RNA sequencing was performed for
397 two technical replicates of four conditions (oxidative stress-prone VSMCs (C2),
398 atheroprotective VSMCs (C3), proatherogenic VSMCs (C4), and untreated VSMCs (C5)),
399 respectively. Approximately 3.8×10^5 cells/well (HAOSMC IV) were seeded in 6-well plates
400 that were covered with a Col I hydrogel (1.5 mg/mL). VSMCs were stimulated as described
401 above for short-read RNA-Seq. Cells were harvested and kept in TRIzol™ reagent (500

402 µL/well, Invitrogen 15596-018). Total RNA was extracted using the RNeasy Plus kit (Qiagen
403 74134). Adaptors were ligated to the 3' and 5' ends of small RNAs, respectively. After
404 hybridization with reverse transcription primer, the first-strand cDNA was synthesized. The
405 double-stranded cDNA library was generated through PCR enrichment. After purification
406 and size selection, libraries with insertions between 18~40 bp were obtained. These libraries
407 were checked with Qubit and real-time PCR for quantification and a bioanalyzer for size
408 distribution detection. Quantified libraries were pooled and sequenced on an Illumina
409 sequencer, targeting 20 million single-end reads of length 50 bases.

410

411 *Small RNA sequencing data analyses*

412 Small RNA-Seq reads were trimmed using cutadapt[33] to identify and trim up to five adapters
413 and remove sequences (i) not containing any adapter, (ii) containing any N's, (iii) shorter
414 than 16 and longer than 28 bases (since no target sequences have this size) (parameters
415 "-a AGATCGGAAGAGCACACGTCT -g GTTCAGAGTTCTACAGTCCGACGATC --max-n 0
416 --discard-untrimmed --minimum-length 16 --maximum-length 28 -n 5"). Trimmed reads were
417 mapped using kallisto[23]. Towards this, mirBase[34] release 22.1 mature miRNA sequences
418 were downloaded from https://www.mirbase.org/download/CURRENT/mature.fa and
419 indexed with k-mer size 13. Subsequently, reads were mapped using kallisto quant with
420 fragment length 20 (-l 20) and length standard deviation 5 (-s 5) as well as parameters
421 "--single --single-overhang".

422 We investigated whether the modified base is part of miRNA seed regions, for which we
423 considered 7mer-m8 sites, *i.e.*, bases 2-8 of the miRNA need to match the reverse
424 complement of the region covering the modified base, which includes 8mer sites having an
425 adenosine as the first base at the target site. The seed regions were obtained from
426 Targetscan[35]
427 (https://www.targetscan.org/vert_80/vert_80_data_download/miR_Family_Info.txt.zip).
428 Annotation of publication-supported miRNA-target interactions was obtained from

429 MirTarBase[36]

430 (https://mirtarbase.cuhk.edu.cn/~miRTarBase/miRTarBase_2025/cache/download/10.0/Micr

431 oRNA_Target_Sites.csv).

432

433 *Proteomics*

434 Quantification of proteins was performed for TGF-β1 (atheroprotective; C3) and PDGF-BB

435 (proatherogenic; C4) stimulated VSMCs using mass spectrometry with four technical

436 replicates each. Proteins (~20 – 44 µg per cell replicate) were extracted with TRIzol

437 according to the manufacturer's recommendation. Protein concentration was determined via

438 µBCA assay (Thermo Scientific 23235) with BSA as a standard. Equal amounts (4 µg) of

439 individual samples were treated with benzonase (0.125 U/µg protein) and subjected to

440 sample preparation, which includes reduction and alkylation, protein precipitation on SP3

441 beads, and digestion with Trypsin/LysC Mix (1:25) overnight at 37 °C. Resulting peptides

442 were subjected to mass spectrometry measurement on a HPLC-ESI-MS/MS system

443 (HPLC=high pressure liquid chromatography, Ultimate 3000 UPLC system;

444 ESI=electrospray ionization) coupled to an Orbitrap Exploris™ 480 mass spectrometer. MS

445 data were analyzed and normalized with the Spectronaut software

446 (https://biognosys.com/software/spectronaut/) using the Uniprot database limited to human

447 entries (v.2023_12). In total, 4,993 proteins were identified with a minimum of two peptides

448 per protein. Only unique and razor peptides were considered. Protein levels represent

449 maxLFQ values (label-free quantification by delayed normalization and maximal peptide

450 ratio extraction). The statistical analysis was performed on the peptide level using the

451 PECA[37] package (version: 1.40.0). A ROTS test (ROPECA approach -

452 reproducibility-optimized peptide change averaging) implemented in the PECA package was

453 used to perform the statistical analysis (https://doi.org/10.1371/journal.pcbi.1005562).

454 Protein set enrichment analysis was conducted using the Enrichr[38] API, with all identified

455 proteins serving as the background (proteins with ≥2 fragments).

456

457 **Results**

458 *Inflammatory VSMC phenotypes are susceptible to enhanced oxidative stress.*

459 To study pro-atherogenic transitions of vascular smooth muscle cells with respect to
460 oxidative stress, gene regulation, and epitranscriptomic changes, we established an *in vitro*
461 cell culture model (**Figure 1A**) according to established protocols. Since VSMCs rapidly
462 transform to a synthetic phenotype if seeded on a plastic surface, we cultured VSMCs on a
463 collagen I hydrogel instead. The contractile, atheroprotective VSMC state was achieved
464 through activation of the TGF-β signaling and then converted to a pro-inflammatory,
465 pro-atherogenic VSMC phenotype by activating PDGF signaling. As we initially
466 hypothesized that endogenous production of reactive oxygen species (ROS) can affect RNA
467 modifications, we screened several combinations of growth factors known to activate
468 mitochondrial activity and hence potentially increase oxidative stress. Whilst the cell number
469 was similar in all conditions (**Figure 1B,** left), enhanced endogenous ROS production
470 assessed by CellROX assays was only observed in a specific VSMC subtype that was
471 primed through treatment with TGF-β1 (5 ng/mL) for four days, followed by PDGF-BB (10
472 ng/mL) / IL-1β (10 ng/mL) treatment for two days, and subsequent extensive PDGF-BB (200
473 ng/mL) stimulation for two hours (condition C1). Enhanced ROS levels were diminished in
474 condition C1 by treatment with 1 mM N-acetylcysteine (NAC), a potent antioxidant (**Figure**
475 **1B,** right). Oxidatively stressed VSMCs showed increased mitochondrial membrane
476 potential as compared to TGF-β1-treated, atheroprotective VSMCs (condition C3) (**Figure**
477 **1C,** left), but similar mitochondrial abundance, indicated by GRP-75 staining **Figure 1C,**
478 right). In contrast, PDGF-BB treatment alone increased both mitochondrial membrane
479 potential and abundance, fostering an energetic state characterized by elevated
480 mitochondrial respiration and glycolytic activity. In contrast, TGF-β1 treatment was
481 associated with a quiescent VSMC state, independent of PDGF-BB stimulation (**Figure 1D**
482 and **Suppl. Figure S1**).

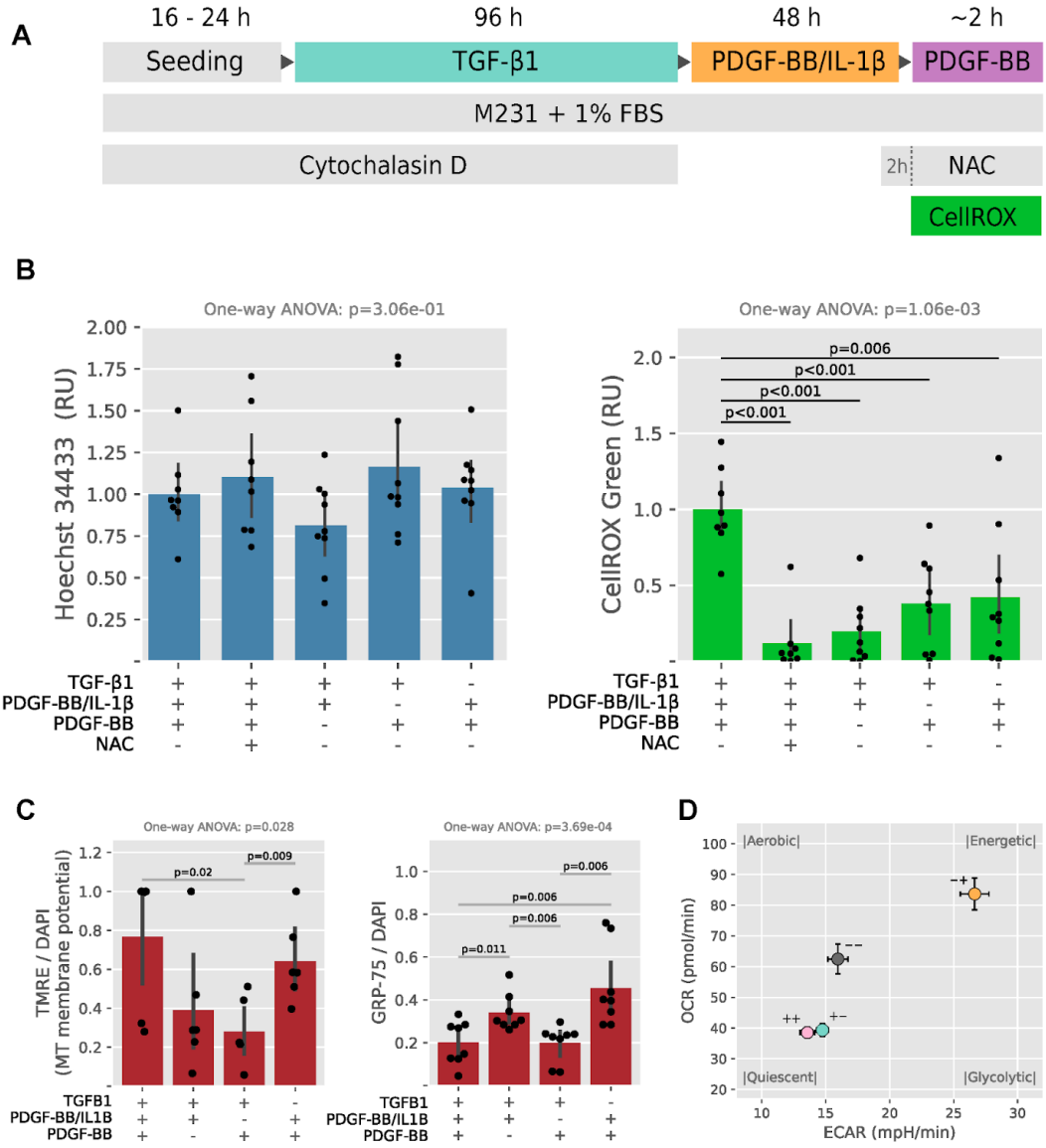

Figure 1: Oxidative stress and mitochondrial activity in vascular smooth muscle cells (SMCs) under atheroprotective (TGF-β1) and pro-atherogenic (PDGF-BB / IL-1β) conditions. (**A**) Cell culture conditions of VSMCs and treatment scheme as described in the Method section (FBS, fetal bovine serum; NAC, N-Acetylcysteine). (**B**) CellROX assays (normalized to nucleus staining with Hoechst 34433) were conducted to assess the endogenous oxidative stress upon treatment with transforming growth factor beta1 (TGF-β1, 5 ng/ml), platelet derived growth factor (PDGF-BB, 10 ng/mL) / interleukin 1β (IL-1β, 10 ng/mL), and high dosage of PDGF-BB (200 ng/mL). NAC (1 mM) was added to counteract oxidative stress. (**C**) The mitochondrial (MT) membrane potential was measured based on TMRE (tetramethylrhodamine ethyl ester perchlorate) fluorescence signal. The abundance of mitochondria was determined by GRP75 antibody staining. Two conditions in **B** and **C** were compared by unpaired Student's t-tests if the one-way ANOVA test was significant ($p<0.05$) over all conditions. (**D**) The oxygen consumption rate (OCR) and extracellular acidification rate (ECAR) of VSMCs treated only with TGF-β1 (+-), or only with PDGF-BB / IL-1β (-+), or with both growth factors (++) were measured with the Agilent Seahorse system. Untreated VSMCs (--) served as control.

498 *Transcriptome profiling of VSMC phenotypes*

499 To identify potential mechanisms by which a specific combination of growth factors and
500 cytokines induces oxidative stress–susceptible VSMCs, we performed global transcriptome
501 profiling of five VSMC states, including atheroprotective VSMCs (TGF-β1; C3),
502 pro-atherogenic VSMCs (PDGF-BB / IL-1β; C4), oxidative stress-prone VSMCs (TGF-β1 >
503 PDGF-BB / IL-1β; C2), oxidatively stressed VSMCs (TGF-β1 > PDGF-BB / IL-1β >
504 PDGF-BB boost; C1), and untreated VSMCs as a control (C5) (**Figure 2A, Suppl. Table S2**
505 **and S3**). PCA of the most variable expressed genes showed the largest variation (PC1)
506 between PDGF-BB / IL-1β-treated VSMCs (C1/C2/C4) and atheroprotective or untreated
507 VSMCs (C3/C5) (**Figure 2B, Suppl. Figure S2**), representing atherogenic pathways. The
508 second largest source of expression variation (PC2) relates to TGF-β1 treatment,
509 representing atheroprotective pathways. Clustering of all five VSMC states identifies elastic
510 fiber formation and extracellular matrix organization (ECM) as key biological processes
511 characterizing mesenchymal-like, atheroprotective VSMCs (TGF-β1; C3) that are shown to
512 contribute to fibrous cap formation in atherosclerotic plaques[3] (**Figure 2C** and **Figure 2D**).
513 On the contrary, pro-athorogenic VSMCs (PDGF-BB / IL-1; C4) exhibit a pro-inflammatory
514 signature, with enhanced expression of genes involved in cytokine-induced signaling,
515 specifically *IL17*, TNF-alpha via NF-κB, and *KRAS*, which were shown to worsen
516 atherosclerosis and accelerate plaque progression.[39,40] Oxidative stress–prone VSMCs (C2)
517 represent an intermediate state between atheroprotective and pro-atherogenic phenotypes,
518 with mesenchymal transition–associated genes remaining inactive while extracellular matrix
519 and inflammatory genes are upregulated (gene clusters 1 and 6; **Figure 2C**). Notably,
520 impairment of mesenchymal transition programs is often associated with reduced cellular
521 adaptability to stress.[41] In parallel, increased ECM production and activation of inflammatory
522 pathways are linked to elevated ROS levels, which promote mitochondrial dysfunction and
523 overwhelm cellular antioxidant systems. Since we suspected high local concentrations of
524 PDGF in atherosclerotic lesions[42], we added very high levels of PDGF-BB to this oxidative

525 stress–prone VMSC phenotype characterized by elevated biosynthetic activity and reduced
526 stress adaptation capacity. Hyperactivation of PDGF signaling resulted not only in elevated
527 ROS levels (**Figure 1B**) but also in reduced expression of many genes essential for cell
528 function and massive upregulation of olfactory receptor genes, which were found to regulate
529 pathophysiological processes in SMCs and described as novel therapeutic targets. [43]

530

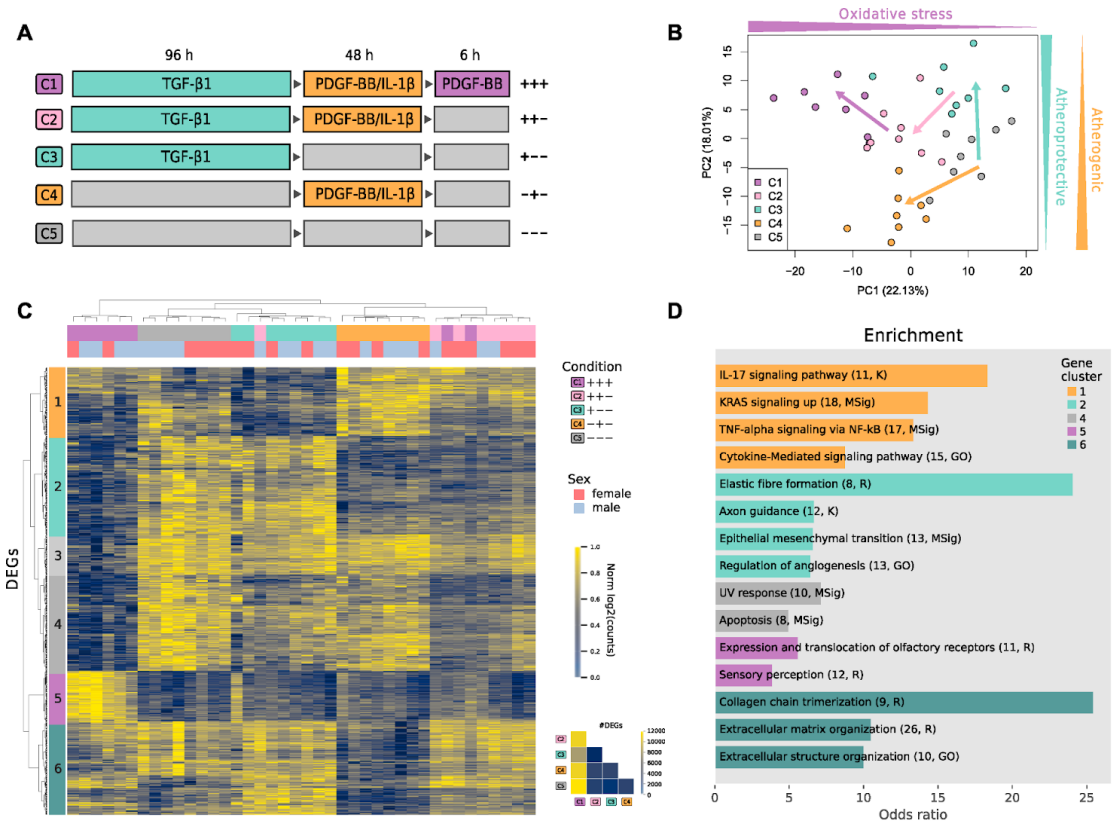

531

532 **Figure 2**: (**A**) Experimental setup relating to the conditions denoted C1-C5 throughout this study. (**B**) Principal
533 component (PC) analysis of five conditions is based on the 1,000 most variable transcripts with normalized and
534 batch-corrected $\log_2$ expression ≥ 5. (**C**) A clustered heatmap shows row-scaled expression of the 1,000 most
535 variable canonical, differential transcripts that differ between conditions (with FDR<=0.001 and mean $\log_2$ count ≥
536 5 in the joint model of all conditions). Up to four top enriched pathways for six gene clusters that are up- or
537 down-regulated in specific conditions are highlighted in (**D**) and colored according to the matching condition.
538

539 In addition to pronounced changes in gene expression (cf. **Supplementary Figure S3**),
540 oxidative stress was also associated with widespread differential splicing. In total, 1,298
541 genes exhibited significant differential splicing in atheroprotective VSMCs (TGF-β1; C3)
542 compared with pro-inflammatory VSMC phenotypes, with *CCL20*, *CXCL8*, *FAH*, and *NOL4L*

543 consistently affected across all comparisons. Among these, *CCL20* isoform switching is the
544 only one with a consequence on protein domain (Chemokine interleukin-8-like domain;
545 InterPro ID IPR001811), where an overall increased expression in pro-atherogenic SMCs
546 was accompanied by an increased usage of the two isoforms that contain the IL8/CXCL8
547 domain (**Suppl. Figure S4A**).
548
549 *Epitranscriptomic profiling of VSMC phenotypes*
550 Next, we used Oxford Nanopore (ONT) direct RNA sequencing in combination with
551 untargeted xPore analysis to obtain a comprehensive overview of the RNA modification
552 landscape that could explain differences in gene expression. In general, up to 4% of mRNA
553 bases of an individual transcript were found to be modified (*e.g.*, methylated) in
554 atheroprotective VSMCs (**Figure 3A** and **Suppl. Table S5**). While the absolute number of
555 modified bases per transcript increases with transcript length, the ratio of modified bases per
556 transcript correlates positively with ONT mRNA abundance but negatively with transcript
557 length. Thus, shorter mRNAs tend to have a higher density of modified bases while
558 expressed at higher levels.
559 Comparison of atheroprotective VSMCs (C3) and pro-atherogenic VSMCs (C4) yielded the
560 largest number of detectable mRNA modification sites (2.1 million in C3 vs. C4), from which
561 5,989 high-confidence differentially modified RNA bases (DMRs) were identified after
562 multiple-testing correction (FDR ≤ 0.05; **Suppl. Table S6** and **S7**). Subsequent filtering for a
563 differential modification rate of at least 25% kept 2,186 differential sites. These DMRs most
564 likely reflect multiple modification types affecting adenosine, cytidine, and uridine (**Suppl.**
565 **Figure S5**). Unexpectedly, we did not find evidence that the endogenous induction of
566 oxidative stress is associated with increased RNA oxidation represented by 8-oxoGuo.
567 Moreover, we found fewer differentially modified mRNA sites (n=1,220) when comparing
568 atheroprotective VSMCs (C3) with oxidatively stressed VSMCs (C1) (**Suppl. Table S8**).
569

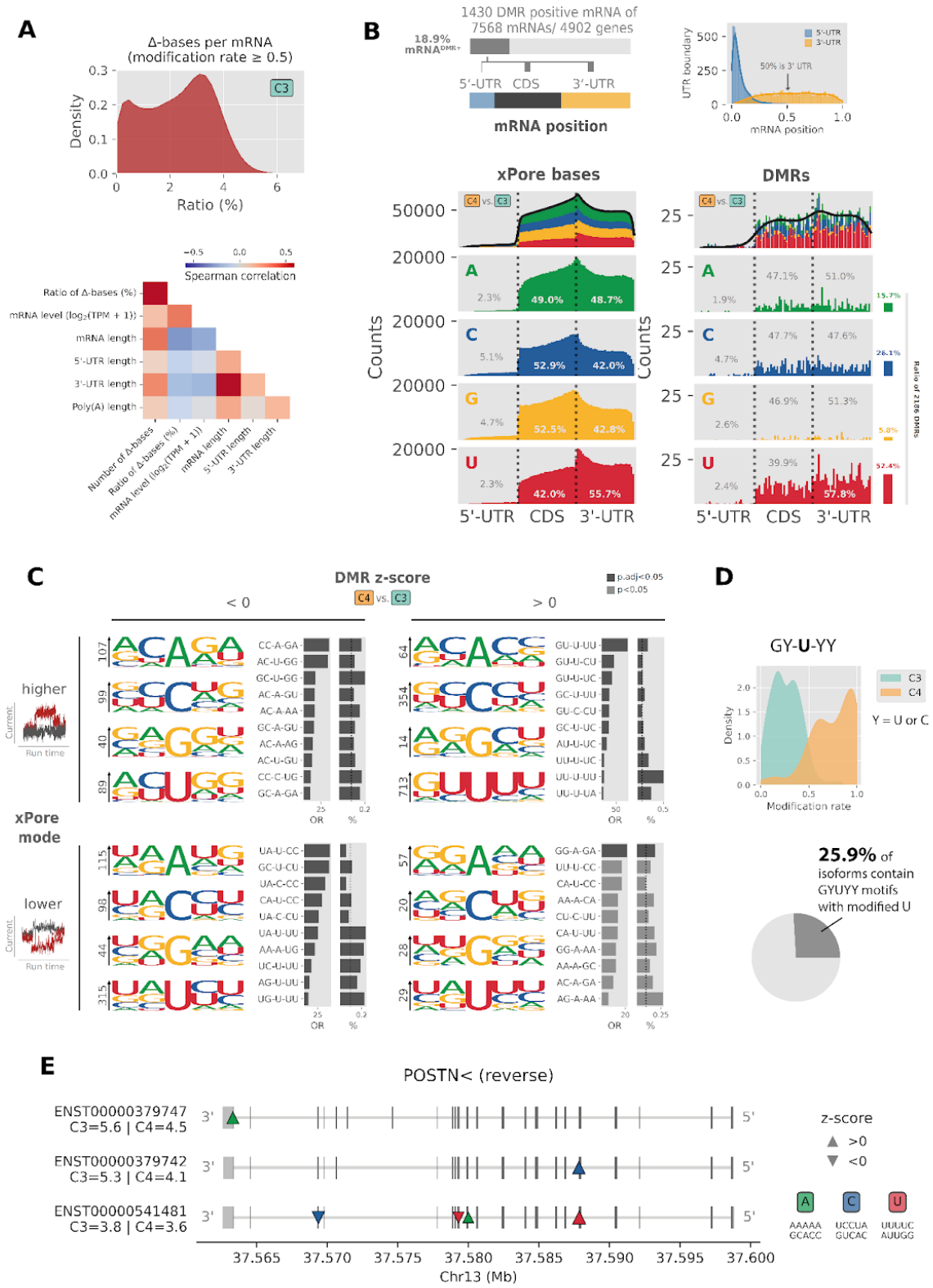

Figure 3: Detection of modified RNA bases with ONT direct RNA sequencing and xPore in vascular smooth muscle cells treated with atheroprotective growth factors (TGF-β1, C3) or pro-inflammatory cytokines (PDGF-BB / IL-1β, C4). Approximately 4 million base positions on 7,568 transcripts were evaluated with xPore. (**A**) The ratio of modified (Δ) RNA bases (rate ≥ 0.5) in TGF-β1-treated VSMCs peaks between 2 to 4%. The Spearman correlation matrix shows that the absolute number of Δ-bases positively correlates with the transcript length as well as the length of UTRs. Contrary, the ratio of modified bases is slightly negatively correlated with these

lengths. (**B**) In total, 2,186 significantly differentially modified RNA bases (DMRs) were identified in the untranslated region (UTR) and coding sequence (CDS) on 1,430 transcripts. Upper right panel: the proportion of 3'-UTR of mRNAs can be 50% and higher, whilst the 5'-UTR sequence is much smaller (usually <10%). The relative distribution within UTRs and CDS is shown for all ~4 million analyzed xPore RNA bases (left) and for 2,186 significant DMRs (C4 vs. C3; right) for all four RNA bases (A, C, G, and U). (**C**) RNA sequence motif analysis highlights the GUUUU motif in which the modification rate of uridine is higher in C4 (DMR z-score > 0). The xPore mode "higher" indicates an increased Nanopore current due to the modified base. The odds ratio (OR) and percentage (%) of the 10 most abundant sequence motifs (5-mers) are shown next to the motif plots. (**D**) Distribution of modification rates for the middle base U of GY-U-YY motifs (p.adj < 0.05 and rate ≥ 0.25), which are modified in ~26% of all DMR-positive mRNA. (**E**) Transcripts of *POSTN* demonstrate that different DMRs can be identified in several isoforms.

Instead, we observed that PDGF-BB treatment led to enhanced modification of uridines in pro-athorogenic VSMCs (PDGF-BB / IL-1β; C4) as well as oxidatively stressed VSMCs (TGF-β1 > PDGF-BB / IL-1β > PDGF-BB boost; C1) (**Figure 3B-D** and **Suppl. Figure S6**). Uridine modifications often occurred in GY-U-YY motifs, with Y being a pyrimidine base (C or U). Thereby, GUUUU was the most prevalent 5-mer context (209 DMR sites in 194 transcripts), showing ~80-fold enrichment across all mRNA sequences analyzed with xPore (**Figure 3C**). Affected genes appear to be regulated by the transcription factors TCF-21, JUN (c-Jun) or JunD and are enriched for epithelial-mesenchymal transition, immune system, cell migration, and the PI3K/AKT/mTOR signaling pathway (**Suppl. Table S9**). Analysis with xPore revealed that many transcripts harbor multiple differentially modified sites, and co-modification of uridine together with adenosine and/or cytidine was frequently observed (cf. **Suppl. Table S10**). Overall, the comparison of atheroprotective VSMCs (C3) and pro-atherogenic VSMCs (C4) yielded 1,258 genes expressing transcripts that contain one or more DMR-sites, with the top affected genes *FN1* (18 sites, 9 transcripts), *ITGB1* (15 sites, 12 transcripts), *HDLBP* (13 sites, 3 transcripts), and *TUBB* (10 sites, 5 transcripts) (cf. **Suppl. Table S11**). Of note, *FN1* and *ITGB1* are described to be major regulators of VSMCs.[44] Other DMR-affected genes and transcripts involved in VSMC-relevant processes are highlighted in **Suppl. Table S12** and **Suppl. Figure S7**. Except *COL6A2* and *PXDC1* (**Suppl. Figure S4B** and **S4C**), none of these notably DMR-affected genes is among the 272 genes for which significant differential splicing was detected between atheroprotective and pro-atherogenic VSMCs (**Suppl. Table S4**).

611 *Association of base modification with protein abundance*

612 Since we detected the largest number of DMRs when comparing atheroprotective (TGF-1β;
613 C3) with pro-atherogenic VMCs (PDGF-BB / IL1-β1; C4), we subsequently quantified the
614 proteome of these VSMCs phenotypes (**Suppl. Table S13**), resulting in 4,995 identified
615 proteins of which 1,171 were significantly differentially abundant after multiple testing
616 correction (**Suppl. Table S14**). Enrichment analysis confirms the pro-inflammatory signature
617 of PDGF-BB / IL1-β1-treated VSMCs (**Figure 4A**). In order to investigate a potential role of
618 RNA modifications on protein levels, we focused on transcripts detected at a minimum of 10
619 transcripts per million (TPM) in both Illumina and ONT sequencing. At this threshold,
620 log10-transformed RNA levels derived from Illumina and ONT correlate best, with a
621 Pearson's correlation coefficient of r=0.66 for C3 and r=0.67 for C4 (cf. **Suppl. Figure S8**),
622 which is within ranges reported previously[45]. In addition, transcript counts were aggregated
623 per gene since proteomics is not isoform-sensitive. Protein levels align with gene expression
624 levels in atheroprotective VSMCs (TGF-1β; C3) when only non-zero values are considered,
625 and this relationship is independent of the presence of differentially modified RNA bases
626 (DMRs in C4 vs. C3). However, DMRs are more frequently identified at higher gene/protein
627 levels (**Figure 4B**). Notably, the proportion of DMR-positive mRNAs decreases from
628 approximately 22% among mRNAs with detectable protein to about 8% among those for
629 which no corresponding protein was detected - despite comparable mRNA levels -
630 suggesting that some DMRs may be crucial for translation activity. Moreover, for genes
631 linked to more than three DMRs, changes in transcript abundance were strongly mirrored at
632 the protein level. This is reflected by a strong correlation between the $\log_2$(fold change) in
633 gene expression and the corresponding $\log_2$(fold change) in protein abundance. (**Figure**
634 **4C**). This relationship supports a role for DMRs in shaping transcriptional programs that
635 extend to protein expression, particularly for genes linked to the TCF21-regulated
636 atheroprotective, fibroblast-/mesenchymal-like VSMC state (C3). A subset of these genes is
637 downregulated during the transition to the pro-inflammatory VSMC phenotype (C4). An

overview of genes with notable differences in corresponding protein levels is shown in **Figure 4D**. Neither the relative position of DMRs within UTRs or coding sequences nor the direction of modification changes suggests a consistent rule governing DMR-dependent transcriptional or translational regulation. Nonetheless, we observe a trend toward reduced adenosine modification (z-score < 0) in genes exhibiting higher protein abundance in pro-atherogenic VMCs, and the opposite trend in genes with lower protein abundance. Moreover, cytidines appear to be differentially modified more frequently when located in the 5'-UTR of genes associated with increased protein levels.

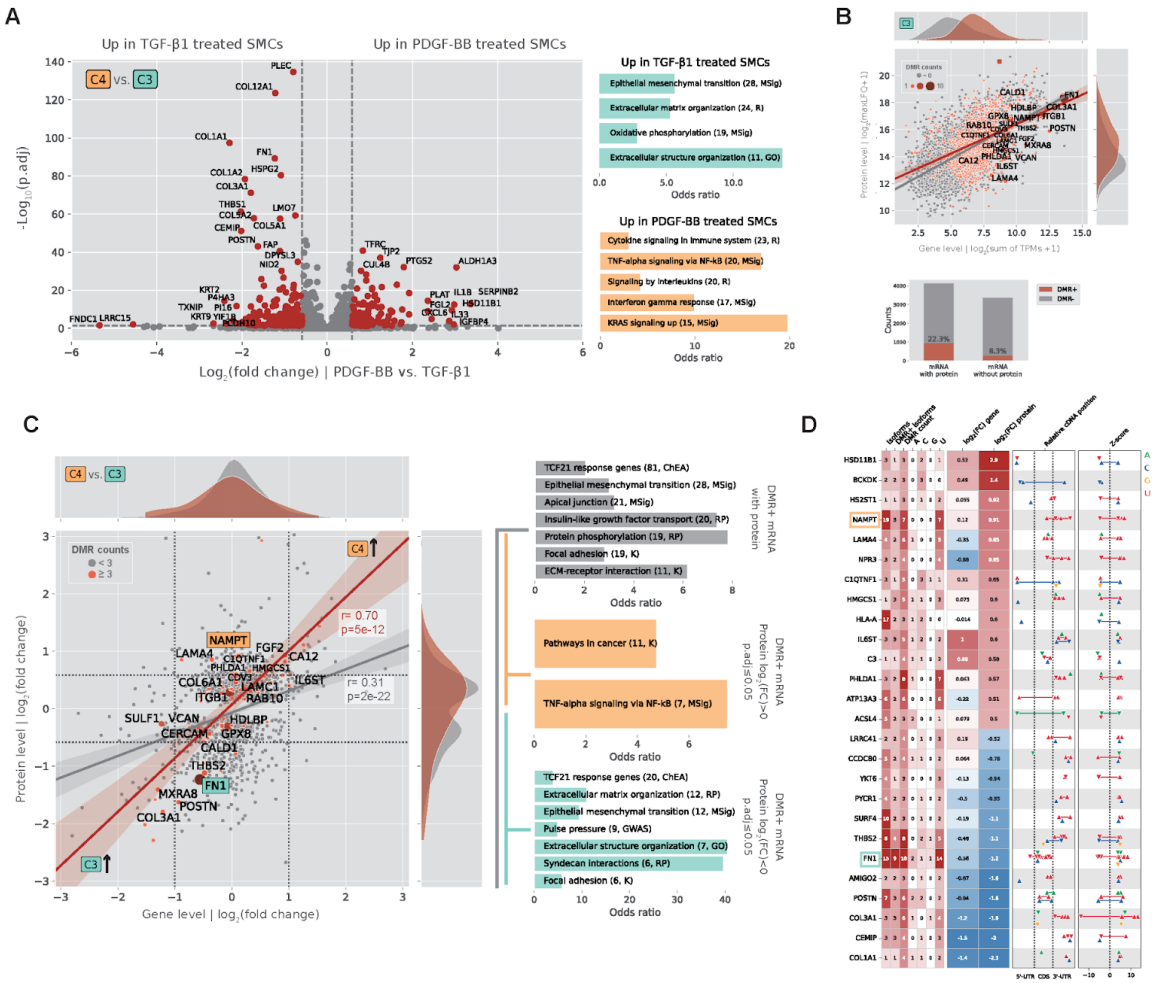

Figure 4: Impact of RNA base modifications on translational activity in atheroprotective and atherogenic smooth muscle cells. (**A**) Differential proteome analysis of cell lysate from vascular smooth muscle cells treated with TGF-β1 (C3) or PDGF-BB / IL-1β (C4) (n=4 replicates per condition). The Vulcano plot and enrichment plots show typical marker proteins and biological processes of TGF-β1 or PDGF signaling. Numbers in parentheses reflect the number of overlapping genes and libraries used are as follows: GO=Gene Ontology; MSig=Molecular Signature database; R=Reactome database. (**B**) Regression plot of gene level (> 0) versus protein level (> 0) of transcripts in C3 with (red) and without (gray) differentially modified RNA bases (DMRs) in C3 vs. C4. The size

654 indicates the number of DMRs across all isoforms per gene. DMR-positive genes with detectable protein account
655 for 22%. The ratio drops to 8.3% if no protein is detected. (**C**) Same as (**B**), as log2-fold changes (FC) for C3
656 versus C4. The Pearson correlation (r) was calculated for genes with ≥ 3 DMRs across all isoforms and < 3
657 DMRs. Gene set enrichment analysis was performed for all genes with ≥ 3 DMRs (gray), and for genes with
658 corresponding protein level $\log_2$(fold change) > 0 (orange), or $\log_2$(fold change) < 0 (turquoise). In addition to (**A**),
659 more gene-set libraries were significant after adjusting for multiple testing: ChEA=ChIP-X enrichment analysis;
660 GWAS= GWAS catalog; K; KEEG database; RP = Reactome Pathways. (**D**) Overview of genes with
661 abs($\log_2$(FC)) > 0.5 (FC=fold change), with differences between gene $\log_2$(FC) and protein $\log_2$(FC) above 0.25,
662 and with more than two identified DMRs across all DMR+ isoforms. The number of isoforms was extracted from
663 Ensembl/ BioMart (release 113). The relative position in untranslated regions (UTR) or coding sequence (CDS)
664 and z-scores (C4 vs. C3) are shown for all bases (A in green, G in yellow, C in blue, and U in red). The xPore
665 mode is indicated as arrows ("higher"=up, "lower"=down).
666

667 *Transcriptomic landscape of mRNA modification–related genes*

668 Since uridine was the most frequently modified RNA base, we first examined the expression
669 level of pseudouridine synthase genes in atheroprotective and pro-atherogenic VSMCs. We
670 observed modest yet significant downregulation of three of them, but only in PDFG-treated,
671 oxidatively stressed VSMCs (C1) (**Suppl. Figure S9**). In contrast, a notable increase in
672 *PUS7* level was observed in pro-atherogenic VMCs, reaching nominal significance (p =
673 0.022, p.adj = 0.098) (**Figure 5A**). Among all mRNA modification–related genes (median
674 $\log_2$(normalized counts) > 5; cf. **Suppl. Table S15**), significant differences between
675 atheroprotective and pro-atherogenic VSMCs were detected only for *TET1* (hm5C oxidase)
676 after adjustment for multiple testing (p.adj. < 0.05). Although it appears that only a few
677 mRNA modifiers and genes encoding for mRNA-binding proteins differ individually, the
678 global expression signatures clearly separate the two VSMC phenotypes (**Figure 5B**),
679 suggesting an orchestrated program of mRNA modification–related genes that promote
680 either atheroprotective or pro-atherogenic pathways.
681

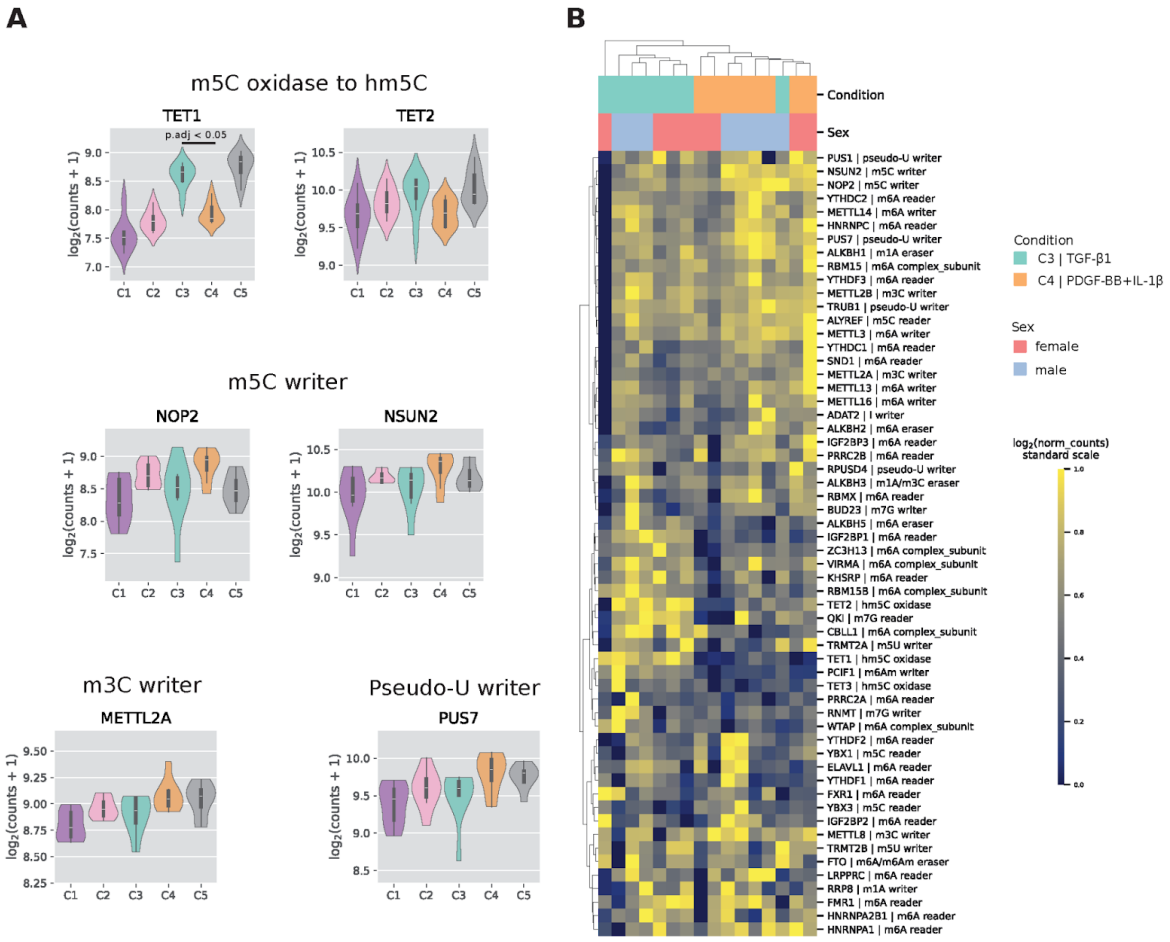

Figure 5: Expression pattern of genes encoding mRNA-modifying enzymes in atheroprotective (C3) and pro-atherogenic (C4) VSMCs. (**A**) Violin plots of genes whose canonical transcripts are differentially expressed in C3 vs. C4 at nominal significance ($p < 0.05$; for *TET1*: p.adj < 0.05; **Suppl. Table S3)**. (**B**) The clustermap shows the standardized expression level of genes with median $\log_2$(normalized counts) ≥ 5 (**Suppl. Table S15**).

RNA base modifications influence poly(A) tail dynamics

Next, we examined how DMRs influence mRNA processing and translational regulation, including poly(A) tail dynamics. Density plots of poly(A) tail lengths in atheroprotective (TGF-1β; C3) and pro-atherogenic VMCs (PDGF-BB / IL1-β1; C4) reveal that genes/transcripts with increasing numbers of DMRs exhibit progressively longer poly(A) tails, along with more pronounced differences between the two VSMC phenotypes (**Figure 6A**). In addition, we observed a strong correlation between gene/protein $\log_2$ fold changes and corresponding shifts in poly(A) tail length. Longer poly(A) tails appear to be associated with lower mRNA levels as well as protein levels in pro-atherogenic VSMCs (**Figure 6B**).

This relationship is highlighted for *NAMPT* and *FN1* in **Figure 6C,** which were the only ones with significant differences in poly(A) tail length after adjusting for multiple testing (cf. **Suppl. Table S16**). While *NAMPT* shows higher expression in pro-atherogenic VSMCs (C4), accompanied by shorter poly(A) tails, *FN1* exhibits the opposite pattern when all isoforms are considered. Interestingly, several uridines show increased modification rates (in "higher" xPore mode) in pro-atherogenic VSMCs. These modified uridines are located predominantly in the 3′-UTRs of *NAMPT* isoforms, whereas in *FN1* isoforms they occur exclusively within coding sequences.

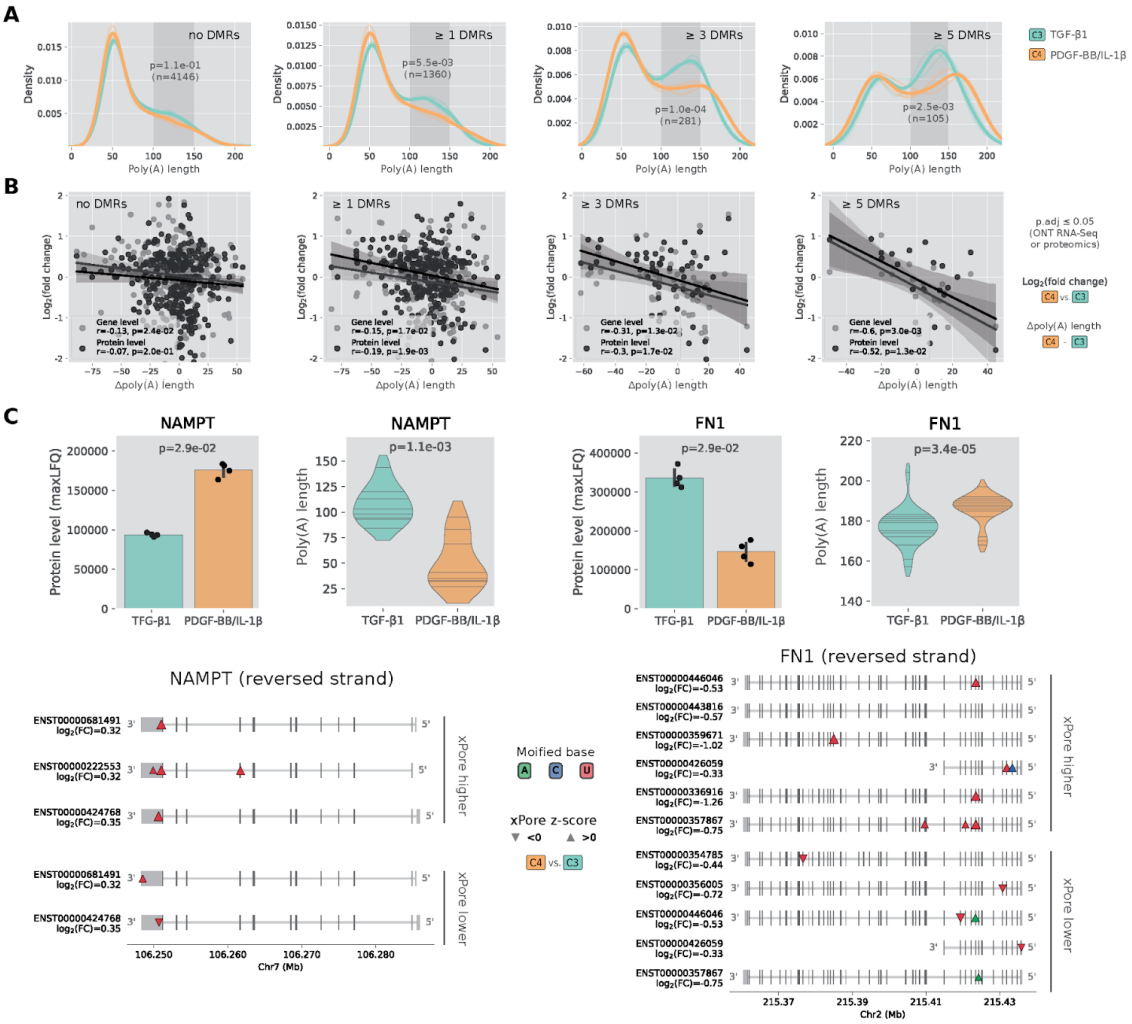

Figure 6: Poly(A) tail length distribution of mRNAs isolated from TGF-β1- (C3) or PDGF-BB / IL-1β-stimulated vascular smooth muscle cells (C4). (**A**) Kernel density plots show increasing poly(A) tail length and greater differences between C3 and C4 with increasing number of differentially modified RNA bases (DMRs). Statistical significance was calculated using a permutation test for the region 100 to 150 adenosines. The number of

transcripts is shown in parentheses. (**B**) Pearson correlation plots of difference (Δ) in poly(A) tail length versus log_2(fold change) for differentially expressed genes/proteins between C3 and C4 (p.adj ≤ 0.5). (**C**) Examples which demonstrate the potential relationship between protein levels (in maxLFQ), poly(A) tail lengths, and the location of DMRs. Mann-Whitney U tests were performed to calculate statistical significance. The poly(A) tail length across all isoforms and replicates (n=3) with a coverage > 10 are displayed per gene. The lower panels show isoforms with DMRs separated by the xPore mode "higher" or "lower", which might reflect differentially modified uridines. Log_2(fold change [FC]) for C4 vs. C3 is displayed beneath each Ensembl transcript ID.

Modified uridine bases are enriched in accessible RNA secondary structures in the 3'-UTR

Next, we predicted RNA secondary structures of 150-nucleotide sequences containing DMR sites using the ViennaRNA library to investigate whether DMRs might be found more frequently in distinct structural elements. In brief, 65 controid RNA secondary structures were predicted per transcript and DMR position by shifting a 150 nucleotide window two bases downstream, starting from 140 nucleotides upstream of the DMR position. Centroid RNA secondary structures were clustered based on similarity scores. The RNA secondary structure with the lowest MFE of the most representative cluster (selected upon cluster size, median MFE, and MFE variance) was taken for over-representation analysis (**Figure 7A**). As part of our quality control, we examined the negative minimal free energy (MFE) of all predicted centroid RNA secondary structures across relative cDNA positions. Consistent with previous observations, the negative median MFE per position declines toward the 3′-UTR, accompanied by reduced GC content, a hallmark of functional mRNAs[46] (**Figure 7B**). Over-representation analysis of DMRs in RNA secondary structure elements revealed that differentially modified uridines are 1.7-fold enriched in interior loops in 3'-UTRs (**Figure 7C** and **Suppl. Table S17**).

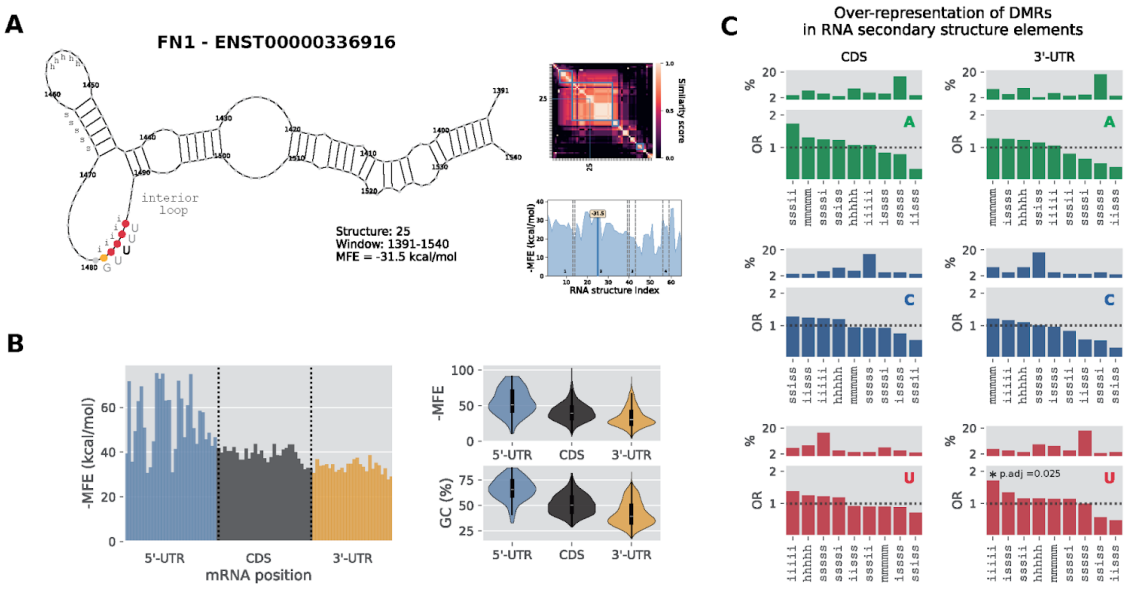

Figure 7: Localization of modified RNA bases (DMRs) in secondary RNA structures. (**A**) Per transcript and DMR, 65 RNA sequences with 150 bases were created by shifting the sequence iteratively by two bases, starting -10 bases upstream. The centroid RNA structure and minimal free energy (MFE) were predicted using the ViennaRNA library. After hierarchical clustering based on pair-wise similarity scores, RNA secondary structure elements as 5-mers (e.g., *hhhhh* for hairpin loop or *sssss* for stacked stem) were extracted from the centroid sequence with the lowest MFE from the largest cluster with the lowest mean cluster-MFE. (**B**) Mean MFE per binned relative DMR positions (90 bins) in 5'/3'-UTR (untranslated region) and coding sequence (CDS). The violin plots highlight the correlation of MFE and GC-content. (**C**) Differentially modified uridines are enriched in predicted interior loops (iiiii) in 3'-UTR. Bar plots show the relative abundance (in %) and odds ratio (OR) of RNA secondary structure elements (*cf.* **Suppl. Table S17**).

Modified RNA bases may modulate miRNA binding

Moreover, we detected an excess of modifications near stop codons at the beginning of the 3'-UTR (*cf.* **Figure 3B**), which has also been reported previously by the authors of xPore[8]. We hypothesize that this enrichment is related to DMRs that influence miRNA binding, as miRNA-to-mRNA binding is reported to be most effective when occurring at the beginning or the end of long 3′-UTRs.[47] Therefore, we assessed the potential impact of DMRs on miRNA binding. We quantified miRNA expression in four VSMC states (C2 to C5) and screened highly expressed miRNAs ($\log_2$(count) ≥ 10 in one replicate) for miRNA-binding sites based on direct 8-mer seed matches. We identified 60 of the 202 highly expressed miRNAs whose seed sequences could directly bind to DMR-containing mRNA regions in 3'-UTR (**Figure 8A** and **Suppl. Table S18**). The highest number of DMR binding sites was detected for miR-494-3p (n = 6), followed by miR-186-5p, miR-200b/c-3p, and miR-28-3p (n = 4) (**Figure**

760 **8B**). DMR-miRNA pairs were found for 85 mRNAs and 104 DMRs, thereby affecting about
761 6% of all DMR-positive transcripts. Of those, 58 sites have uridine modified, 28 cytidine, 15
762 adenosine, and 3 guanosine (**Figure 8A**). However, miRNA binding for only six genes had
763 experimental evidence and a respective publication recorded in the miRTarBase database.
764 In addition, the specific binding site of miR-493-5p at the unique DMR-site AA-A-UG of
765 *ITGB1-204* in 3'-UTR (cDNA position 2859) was the only one experimentally confirmed[48],
766 but not yet recorded in miRTarBase. **Figure 8C** illustrates a possible miRNA binding model
767 postulating that miR-493-5p directly binds to a modified adenosine located in the AA-A-UG
768 sequence. Another DMR site (GU-U-UC) is located about 230 nucleotides downstream at
769 the tip of a hairpin loop. Interestingly, the mRNA levels are similar in atheroprotective
770 (TGF-1β; C3) and pro-atherogenic VMCs (PDGF-BB / IL1-β1; C4), yet integrin β1 protein
771 levels appear to be higher in the latter VMC phenotype. In this model, elevated uridine
772 modification in pro-atherogenic VMCs, particularly within a hairpin loop, could promote
773 mRNA stability or reinforce RNA structural integrity. Conversely, decreased adenosine
774 modification may reduce miRNA-binding efficiency, thereby limiting miRNA-mediated
775 translational repression. Notably, the miRNA context-binding sequence is conserved across
776 all *ITGB1* isoforms, where modified uridines or adenosines lie nearby (**Figure 8D**).
777 In order to investigate whether increased levels of miRNAs can influence RNA base
778 modification, *e.g.*, by decorating the modifiable site, we profiled the mirNOME in phenotypic
779 transition conditions C2 to C5 (**Suppl. Table S19** and **S20**). In total, 131 miRNAs were
780 significantly differentially expressed across all four conditions, with the top four being
781 miR-145-5p, miR-204-5p, miR-146a-5p, and miR-5585-3p. Thereby, miR-145-5p showed
782 the greatest expression difference, exhibiting a ~4-fold higher abundance in TGF-β1-treated
783 VSMCs (C3) compared with PDGF-BB / IL-1β-treated VSMCs (C4) (**Suppl. Table S20**). This
784 is consistent with prior studies demonstrating time- and dose-dependent downregulation of
785 miR-145-5p under PDGF stimulation.[49] However, neither for miR-145-5p nor the other

differentially expressed mRNAs did we find evidence that miRNA binding directly affects RNA base modifications at specific miRNA binding sites.

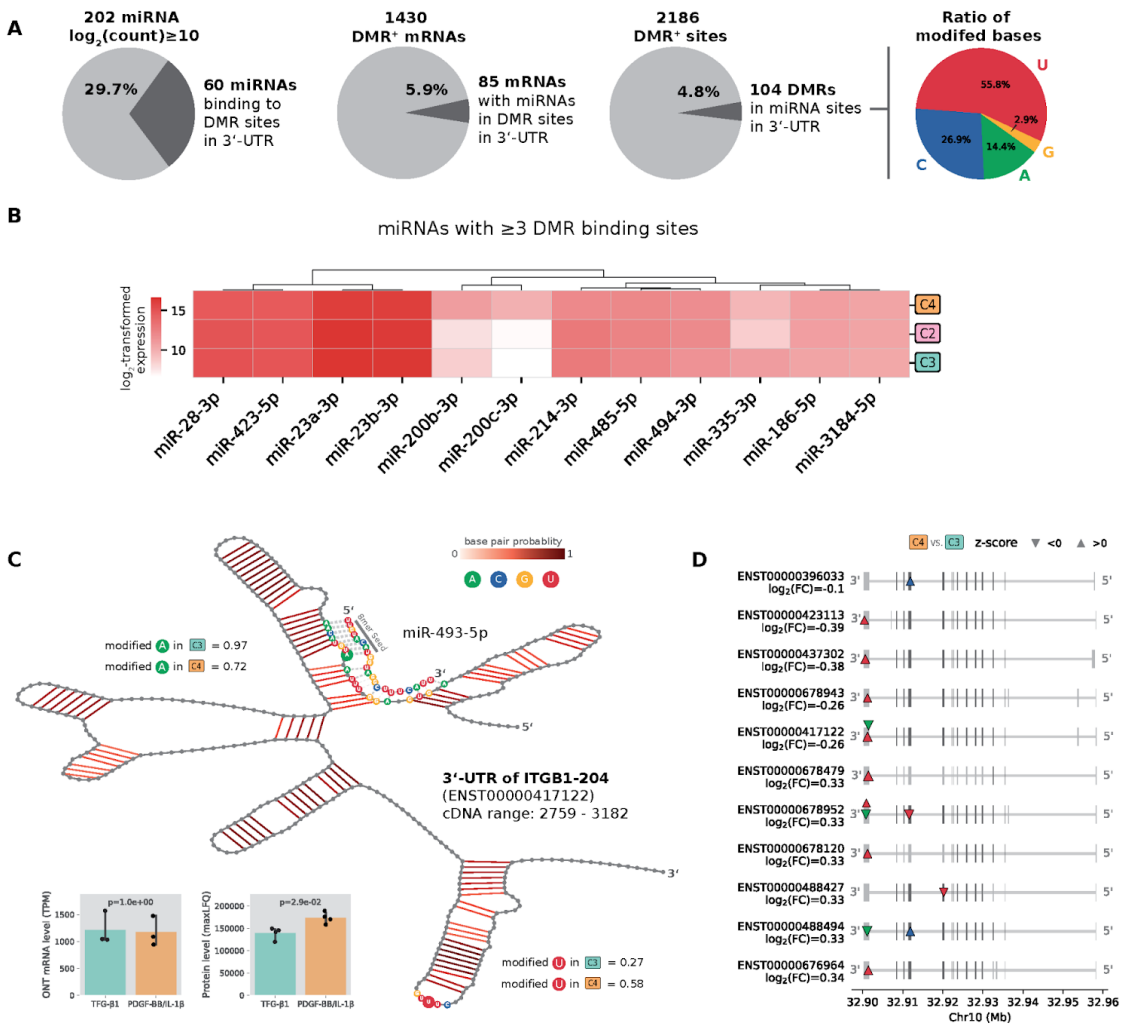

Figure 8: Potential binding of miRNAs at differentially modified RNA bases (DMRs). (**A**) The left pie chart illustrates that 60 of the 202 highly expressed miRNAs (log_2 count ≥ 10) are predicted to interact with DMRs through the 8-mer seed sequence. The ratio of DMR-positive transcripts and DMRs at miRNA binding sites in 3'-UTR is shown in the middle. The right pie chart displays the ratio of modified bases in predicted miRNA binding sites. (**B**) Expression pattern of highly expressed miRNAs with more than three predicted DMR binding sites across three conditions (C2=TGF-β1 > PDGF-BB / IL-1β, C3=TGF-β1, C4=PDGF-BB / IL-1β). (**C**) The isoform ITGB1-204 serves as an example in which a modified adenosine has been identified in a confirmed miRNA binding region for miR-493-5p[48]. A reduced modification rate in PDGF-BB / IL-1β-treated smooth muscle cells (C4=0.72 vs. C3=0.97) is associated with an increased integrin beta-1 protein level (ITGB1). A second DMR was identified downstream, where enhanced uridine modification was measured via xPore (C4=0.58 vs. C3=0.27). (**D**) DMRs across all DMR-positive isoforms of ITGB1 (color code as in B). Log_2(fold change [FC]) is shown for C4 versus C3 below the Ensembl transcript ID. Upward triangles represent a modification increase, downward triangles a decrease.

Discussion

Using Nanopore direct RNA-Seq, we performed a transcriptome-wide, untargeted screening of RNA base modifications in vascular smooth muscle cells (VSMCs) under atheroprotective (TGF-β1) and pro-atherogenic (PDGF-BB / IL-1β) treatment. Our main findings are that 1) up to 5% of mRNA bases appear to be modified (*e.g.*, methylated). 2) Differences in mRNA base modifications between atheroprotective and atherogenic VSMC phenotypes often occur near stop codons and at the beginning of 3'-UTRs, specifically affecting uridines in accessible 3'-UTR regions. 3) The G-Y-U-YY (with Y=U/C) is the most prominent motif found in ~26% of isoforms. 4) Differentially modified RNA bases might be explained by global changes in RNA-modifying enzyme levels. 5) DMRs might be linked to translation activity, *e.g.,* by regulating Poly(A) tail dynamics and miRNA binding.

These findings expand the understanding of VSMC phenotype switching in the context of atherosclerosis beyond transcriptional and epigenetic regulation.[5] Although we were not able to detect traces of mRNA oxidation in oxidatively stressed VSMCs using Nanopore direct RNA-Seq, our multi-level analysis suggests that mRNAs can harbor multiple types of base modifications. Further, pro-inflammatory cytokines can influence the epitranscriptomic landscape by altering the expression levels of RNA-modifying enzymes. For example, nominally significant shifts in mRNA abundance for the pseudouridine writer *PUS7* and several m^5C modifiers (*TET1*, *TET2*, *NOP2*, *NSUN2*) may explain the higher rate of uridine and cytidine modification in pro-atherogenic VMCs detected by xPore. However, the molecular mechanisms and temporal dynamics underlying cytokine-induced regulatory programs that involve several classes of mRNA-modifying enzymes are largely unresolved. In particular, the signaling pathways and transcription factors that control the expression of specific mRNA-modifying enzymes, the stability of these enzymes under defined conditions, and the kinetics of base modification on endogenous mRNAs remain to be elucidated.

The most strongly enriched sequence context was the GY-U-YY motif (Y = pyrimidine base, C or U). To our knowledge, this motif has not been described so far. Our

832 epitranscriptome-wide analyses suggest that modification of uridine may foster the
833 PI3K/AKT signaling pathway triggered by PDGF stimulation[50] by stabilizing transcripts
834 essential for this pathway while destabilizing transcripts associated with antagonistic
835 pathways. For example, many uridine-modified transcripts downregulated in pro-atherogenic
836 VSMCs are under the control of the transcription factor TCF21, which normally suppresses
837 PI3K/AKT signaling.[51] TCF21 is known as a key driver of VSMC state transitions in
838 atherosclerosis[2,] and the fact that many base-modified transcripts are regulated by TCF21
839 highlights the importance of mRNA base modifications in atherosclerosis.

840 To elucidate regulatory mechanisms underlying differentially modified RNA bases (DMRs),
841 we investigated multiple possible consequences of DMRs on mRNA processing. We
842 analyzed the impact of DMRs on mRNA splicing but did not find evidence for
843 pathway-relevant differences in isoform usage in a DMR-dependent manner. In fact, DMRs
844 were often found in proximity to stop codons in agreement with previous studies[8,52],
845 indicating rather regulatory activity that might impact mRNA usage, mRNA folding, mRNA
846 stability, or miRNA binding, and thus translational output.

847 First, we observed a negative correlation of protein abundance and poly(A) tail lengths,
848 particularly for transcripts harboring DMRs, which is in line with a previous study that also
849 applied Nanopore direct RNA-Seq[52]. The potential contribution of DMRs highlights, indeed,
850 the regulatory potential of these modifications.

851 Second, uridine modifications were enriched in predicted single-stranded RNA structure
852 elements in 3'-UTRs, supporting the regulatory nature of these mRNA modifications, as
853 these regions are potentially accessible for RNA-modifying enzymes and allow binding of
854 proteins that exert post-transcriptional regulatory effects. The vast majority of significantly
855 differential modifications affected uridine, likely representing pseudouridine (Ψ), which is the
856 most common RNA modification. For Ψ, both stabilizing and destabilizing effects on mRNA
857 were described[53], and the examples of *NAMPT* and *FN1* hint that uridine modification in
858 3'-UTRs might be associated with enhanced mRNA stability and increased translational

859 output (*cf. NAMPT*), whereas uridine modification within coding sequence could potentially
860 have opposite consequences (*cf. FN1*).
861 Third, it has been demonstrated that mRNA modifications can modulate miRNA binding
862 when located in seed match regions in 3′-UTR miRNA binding sites.[54] Notably, 60 out of 202
863 highly expressed miRNAs could directly bind to DMRs with their seed sequence, and
864 modified uridine accounts for ~56% of all affected DMR-sites. Although none of the
865 predicted uridine modification-related miRNA binding sites were experimentally validated
866 according to miRTarBase, we hypothesize that some of the identified uridine modifications in
867 3′-UTR can weaken miRNA binding and thereby prolong mRNA half-life and promote
868 translational output. Nonetheless, additional in-depth studies are required to elucidate the
869 regulatory implications of uridine modifications. Since some of the DMR-related miRNAs are
870 directly related to SMC biology and atherosclerosis (*e.g.*, miR-22, miR-143, miR-145,
871 miR-200, miR-424)[55,56], the notion of mRNA modifications affecting miRNA regulation might
872 help to optimize miRNAs as novel therapeutics.
873 While this study is the first one that comprehensively combines investigations based on
874 short-read sequencing, long-read direct RNA sequencing, as well as mass spectrometry,
875 such multi-platform integration has technical limitations. For example, there is still a
876 discrepancy between short-read RNA-Seq and long-read RNA-Seq with respect to
877 determining expression estimates[57], as well as mapping of reads. Further, quantification of
878 long reads can be affected by incomplete transcript references, and recently, a large number
879 of novel transcripts have been detected in a similar experimental setup to ours[18]. Despite the
880 higher mapping accuracy of long-read sequencing, the limited throughput of MinION flow
881 cells restricted ONT analyses to highly expressed genes that exhibit similar expression
882 levels in two conditions, preventing differential modification testing for many transcripts.
883 Consequently, insufficient coverage and limited replicates likely led to a considerable
884 proportion of missed DMRs, which may explain the low number of detected modifications in
885 oxidatively stressed VSMCs despite differential expression of multiple genes related to

mRNA modification. Moreover, the time point of DMR assessment after cytokine stimulation might be crucial, as some RNA base modifications might lead to rapid mRNA degradation.

A further challenge in assessing the regulatory impact of DMRs on translational output is that the protein quantification relied on peptide-based measurements, which generally permit assignment at the gene level but not at the transcript level, thereby limiting the linkage of isoform-resolved DMRs to protein expression.

Another limitation is the use of the modification-type agnostic detection approach. Although k-mer context and enzyme-related gene expression can suggest specific modification types (e.g., the DRACH motif for m6A), we did not detect strong signals of known sequence motifs at differential sites. Moreover, the ONT RNA002 chemistry precluded the use of ONT basecalling models for specific modifications, which are currently available only for RNA004 chemistry[58] (*cf.* https://genesilico.pl/modomics/tools). Consequently, accurate classification of individual, specific modification types will require dedicated technologies and experimental validation in future studies.

In conclusion, our modification-type-agnostic approach provides a comprehensive, transcriptome-wide view of the RNA modification landscape underlying VSMC phenotypic transitions. We show that distinct RNA modification types frequently co-localize within the same transcripts, particularly near stop codons, suggesting combinatorial regulatory effects on processes such as polyadenylation, mRNA stability, and interactions with regulatory proteins or miRNAs. Moreover, our data indicate that mRNA base modifications – especially uridine modifications – act as post-transcriptional regulators that fine-tune cytokine-induced, transcription factor–specific signaling pathways and help maintain atherosclerosis-relevant SMC phenotypes. Finally, modification sites may serve as targets for miRNA-based therapeutic strategies, and base modifications may be detectable in circulating cell-free RNA, highlighting their potential as biomarkers of disease severity.

Data Availability

Transcriptome sequencing data (Illumina mRNA and small RNA-Seq as well as ONT direct RNA-Seq) for this study have been deposited in the European Nucleotide Archive (ENA) at EMBL-EBI under study accession number PRJEB98980 (https://www.ebi.ac.uk/ena/browser/view/PRJEB98980). Proteomics raw data files are available in PRIDE under accession ID PXD065513. The modification workflow is available at https://github.com/iwohlers/2025_ont_rnaseq_vsmc. Key result files, scripts, and figures are available at FAIRDOMHub under https://fairdomhub.org/projects/461.

Acknowledgments

Initial investigations of the ONT data and of xPore results were performed by Lalitha Kamada as part of her Master's thesis, which was co-supervised by IW and Sven Rahmann and conducted within the Medical Systems Biology Group of Hauke Busch. We are further grateful to Jeanette Erdmann (deceased 2023), former head of the Institute on Cardiogenetics at the University of Lübeck, for supporting the research environment in which this work was conducted. This work used the high-performance computing infrastructure at the Research Center Borstel, Leibniz Lung Center.

Sources of Funding

This work was partially funded by a miniproposal from the Cluster of Excellence Precision Medicine in Chronic Inflammation to TR and IW. Illumina mRNA sequencing was carried out at the Competence Centre for Genomic Analysis (Kiel), which was supported by the DFG Research Infrastructure NGS_CC (project 407495230) as part of the Next Generation Sequencing Competence Network (project 423957469). TZ is funded by the German Centre for Cardiovascular Research (81Z0700107). TZ is co-inventor of an international patent on the use of a computing device to estimate the probability of myocardial infarction

(International Publication No. WO2022043229A1) and is a shareholder in ART.EMIS GmbH Hamburg.

Disclosures

The authors declare that there are no conflicts of interest.

Supplemental Material

Supplement containing Supplementary Methods and Supplementary Figures S1-S9 (PDF)

Supplementary Tables S1-S20 (XLSX)

References

1. Sarraju A, Nissen SE. Atherosclerotic plaque stabilization and regression: a review of clinical evidence. *Nature Reviews Cardiology*. 2024;21(7):487–497.
2. Chen R, McVey DG, Shen D, Huang X, Ye S. Phenotypic Switching of Vascular Smooth Muscle Cells in Atherosclerosis. *Journal of the American Heart Association*. 2023;12(20):e031121.
3. Yap C, Mieremet A, de Vries CJM, Micha D, de Waard V. Six Shades of Vascular Smooth Muscle Cells Illuminated by KLF4 (Krüppel-Like Factor 4). *Arteriosclerosis, Thrombosis, and Vascular Biology*. 2021.
4. Grootaert MOJ, Bennett MR. Vascular smooth muscle cells in atherosclerosis: time for a re-assessment. *Cardiovascular Research*. 2021;117(11):2326–2339.
5. Zurek M, Aavik E, Mallick R, Ylä-Herttuala S. Epigenetic Regulation of Vascular Smooth Muscle Cell Phenotype Switching in Atherosclerotic Artery Remodeling: A Mini-Review. *Frontiers in Genetics*. 2021;12:1449.
6. Huang J, Fu Y. Epigenetic leash on the epitranscriptome: unveiling a novel regulatory axis in vascular smooth muscle contractility. *Cardiovascular Research*. 2025;121(12):1803–1805.
7. Zhang Y, Lu L, Li X. Detection technologies for RNA modifications. *Experimental & Molecular Medicine*. 2022;54(10):1601–1616.
8. Pratanwanich PN, Yao F, Chen Y, Koh CWQ, Wan YK, Hendra C, Poon P, Goh YT, Yap PML, Chooi JY, Chng WJ, Ng SB, Thiery A, Goh WSS, Göke J. Identification of differential RNA modifications from nanopore direct RNA sequencing with xPore. *Nature Biotechnology*. 2021:1–9.
9. Jonkhout N, Tran J, Smith MA, Schonrock N, Mattick JS, Novoa EM. The RNA modification landscape in human disease. *RNA*. 2017;23(12):1754–1769.
10. Nossent AY. The epitranscriptome: RNA modifications in vascular remodelling. *Atherosclerosis*. 2023;374:24–33.
11. Stopa V, Dafou D, Karagianni K, Nossent AY, Farrugia R, Devaux Y, Sopic M, AtheroNET COST Action CA21153 (www.atheronet.eu). Epitranscriptomics in atherosclerosis: Unraveling RNA modifications, editing and splicing and their implications in vascular disease. *Vascular Pharmacology*. 2025;159:107496.
12. Fei J, Cui X-B, Wang J-N, Dong K, Chen S-Y. ADAR1-Mediated RNA Editing, A Novel Mechanism Controlling Phenotypic Modulation of Vascular Smooth Muscle

Cells. *Circulation Research*. 2016;119(3):463–469.
13. Ye W, Gao W, Ho CK, Cui L, Lau JYW, Tian XY, Zhou B, Lui KO. YY1 regulates vascular resistance and blood pressure dynamics through epigenetic control of m6A RNA modifications in vascular smooth muscle cells. *Cardiovascular Research*. 2025;121(12):1898–1916.
14. Poulsen HE, Specht E, Broedbaek K, Henriksen T, Ellervik C, Mandrup-Poulsen T, Tonnesen M, Nielsen PE, Andersen HU, Weimann A. RNA modifications by oxidation: A novel disease mechanism? *Free Radical Biology and Medicine*. 2012;52(8):1353–1361.
15. Li Y, Wang X. The role of DNA and RNA guanosine oxidation in cardiovascular diseases. *Pharmacological Research*. 2024;204:107187.
16. Guan X, Hu Y, Hao J, Lu M, Zhang Z, Hu W, Li D, Li C. Stress, Vascular Smooth Muscle Cell Phenotype and Atherosclerosis: Novel Insight into Smooth Muscle Cell Phenotypic Transition in Atherosclerosis. *Current Atherosclerosis Reports*. 2024;26(8):411–425.
17. Camaré C, Pucelle M, Nègre-Salvayre A, Salvayre R. Angiogenesis in the atherosclerotic plaque. *Redox Biology*. 2017;12:18–34.
18. Wu H, Lu Y, Duan Z, Wu J, Lin M, Wu Y, Han S, Li T, Fan Y, Hu X, Xiao H, Feng J, Lu Z, Kong D, Li S. Nanopore long-read RNA sequencing reveals functional alternative splicing variants in human vascular smooth muscle cells. *Communications Biology*. 2023;6(1):1104.
19. Chen C-N, Li Y-SJ, Yeh Y-T, Lee P-L, Usami S, Chien S, Chiu J-J. Synergistic roles of platelet-derived growth factor-BB and interleukin-1beta in phenotypic modulation of human aortic smooth muscle cells. *Proceedings of the National Academy of Sciences of the United States of America*. 2006;103(8):2665–2670.
20. Saito SY, Hori M, Ozaki H, Karaki H. Cytochalasin D inhibits smooth muscle contraction by directly inhibiting contractile apparatus. *Journal of Smooth Muscle Research = Nihon Heikatsukin Gakkai Kikanshi*. 1996;32(2):51–60.
21. Ezeriņa D, Takano Y, Hanaoka K, Urano Y, Dick TP. N-Acetyl Cysteine Functions as a Fast-Acting Antioxidant by Triggering Intracellular H2S and Sulfane Sulfur Production. *Cell Chemical Biology*. 2018;25(4):447-459.e4.
22. Bray NL, Pimentel H, Melsted P, Pachter L. Near-optimal probabilistic RNA-seq quantification. *Nature Biotechnology*. 2016;34(5):525–527.
23. Pimentel H, Bray NL, Puente S, Melsted P, Pachter L. Differential analysis of RNA-seq incorporating quantification uncertainty. *Nature Methods*. 2017;14(7):687–690.
24. Ewels P, Magnusson M, Lundin S, Käller M. MultiQC: summarize analysis results for multiple tools and samples in a single report. *Bioinformatics (Oxford, England)*. 2016;32(19):3047–3048.
25. Xiao Y, Hsiao T-H, Suresh U, Chen H-IH, Wu X, Wolf SE, Chen Y. A novel significance score for gene selection and ranking. *Bioinformatics (Oxford, England)*. 2014;30(6):801–807.
26. Milacic M, Beavers D, Conley P, Gong C, Gillespie M, Griss J, Haw R, Jassal B, Matthews L, May B, Petryszak R, Ragueneau E, Rothfels K, Sevilla C, Shamovsky V, et al. The Reactome Pathway Knowledgebase 2024. *Nucleic Acids Research*. 2024;52(D1):D672–D678.
27. Kanehisa M, Furumichi M, Sato Y, Matsuura Y, Ishiguro-Watanabe M. KEGG: biological systems database as a model of the real world. *Nucleic Acids Research*. 2025;53(D1):D672–D677.
28. Klopfenstein DV, Zhang L, Pedersen BS, Ramírez F, Warwick Vesztrocy A, Naldi A, Mungall CJ, Yunes JM, Botvinnik O, Weigel M, Dampier W, Dessimoz C, Flick P, Tang H. GOATOOLS: A Python library for Gene Ontology analyses. *Scientific Reports*. 2018;8(1):10872.
29. Vitting-Seerup K, Sandelin A. IsoformSwitchAnalyzeR: analysis of changes in

genome-wide patterns of alternative splicing and its functional consequences. *Bioinformatics (Oxford, England)*. 2019;35(21):4469–4471.

30. Gleeson J, Leger A, Prawer YDJ, Lane TA, Harrison PJ, Haerty W, Clark MB. Accurate expression quantification from nanopore direct RNA sequencing with NanoCount. *Nucleic Acids Research*. 2022;50(4):e19.
31. Li H. Minimap2: pairwise alignment for nucleotide sequences. Birol I, ed. *Bioinformatics*. 2018;34(18):3094–3100.
32. Love MI, Huber W, Anders S. Moderated estimation of fold change and dispersion for RNA-seq data with DESeq2. *Genome Biology*. 2014;15(12):550.
33. Martin M. Cutadapt removes adapter sequences from high-throughput sequencing reads. *EMBnet.journal*. 2011;17(1):10–12.
34. Kozomara A, Birgaoanu M, Griffiths-Jones S. miRBase: from microRNA sequences to function. *Nucleic Acids Research*. 2019;47(D1):D155–D162.
35. Lewis BP, Burge CB, Bartel DP. Conserved seed pairing, often flanked by adenosines, indicates that thousands of human genes are microRNA targets. *Cell*. 2005;120(1):15–20.
36. Cui S, Yu S, Huang H-Y, Lin Y-C-D, Huang Y, Zhang B, Xiao J, Zuo H, Wang J, Li Z, Li G, Ma J, Chen B, Zhang H, Fu J, et al. miRTarBase 2025: updates to the collection of experimentally validated microRNA-target interactions. *Nucleic Acids Research*. 2025;53(D1):D147–D156.
37. Suomi T, Hiissa J, Elo L. PECA: Probe-level Expression Change Averaging.
38. Xie Z, Bailey A, Kuleshov MV, Clarke DJB, Evangelista JE, Jenkins SL, Lachmann A, Wojciechowicz ML, Kropiwnicki E, Jagodnik KM, Jeon M, Ma'ayan A. Gene Set Knowledge Discovery with Enrichr. *Current Protocols*. 2021;1(3):e90.
39. Pan H, Ho SE, Xue C, Cui J, Johanson QS, Sachs N, Ross LS, Li F, Solomon RA, Connolly ES, Patel VI, Maegdefessel L, Zhang H, Reilly MP. Atherosclerosis Is a Smooth Muscle Cell–Driven Tumor-Like Disease. *Circulation*. 2024;149(24):1885–1898.
40. Ma L, Yang W, Gao W, Liu X, Dong M, An G, Meng X. IL-17 as a therapeutic target in cardiovascular diseases: Mechanistic insights and translational opportunities. *Pharmacological Research*. 2025;219:107879.
41. Farahzadi R, Valipour B, Fathi E, Pirmoradi S, Molavi O, Montazersaheb S, Sanaat Z. Oxidative stress regulation and related metabolic pathways in epithelial–mesenchymal transition of breast cancer stem cells. *Stem Cell Research & Therapy*. 2023;14:342.
42. Pang S, Tao Z, Min X, Zhou C, Pan D, Cao Z, Wang X. Correlation between the Serum Platelet-Derived Growth Factor, Angiopoietin-1, and Severity of Coronary Heart Disease. *Cardiology Research and Practice*. 2020;2020(1):3602608.
43. Kalbe B, Knobloch J, Schulz VM, Wecker C, Schlimm M, Scholz P, Jansen F, Stoelben E, Philippou S, Hecker E, Lübbert H, Koch A, Hatt H, Osterloh S. Olfactory Receptors Modulate Physiological Processes in Human Airway Smooth Muscle Cells. *Frontiers in Physiology*. 2016;7.
44. Feil S, Zaldivia MTK, Kiesel J, Roessing M, Peter A, Morales-Cano D, Bentzon JF, Lehners M, Feil R. Smooth Muscle Cell-Derived Fibronectin Promotes an Atheroprotective Smooth Muscle Cell Phenotype Associated With Altered NO-cGMP Signaling. *Journal of the American Heart Association: Cardiovascular and Cerebrovascular Disease*. 2025;14(11):e040395.
45. Mock A, Braun M, Scholl C, Fröhling S, Erkut C. Transcriptome profiling for precision cancer medicine using shallow nanopore cDNA sequencing. *Scientific Reports*. 2023;13(1):2378.
46. Palazzo AF, Kang YM. GC-content biases in protein-coding genes act as an "mRNA identity" feature for nuclear export. *BioEssays*. 2021;43(2):2000197.
47. Grimson A, Farh KK-H, Johnston WK, Garrett-Engele P, Lim LP, Bartel DP. MicroRNA targeting specificity in mammals: determinants beyond seed pairing.

Molecular Cell. 2007;27(1):91–105.
48. Liang Z, Kong R, He Z, Lin L-Y, Qin S-S, Chen C-Y, Xie Z-Q, Yu F, Sun G-Q, Li C-G, Fu D, Jiang G-X, Chen J, Ma Y-S. High expression of miR-493-5p positively correlates with clinical prognosis of non small cell lung cancer by targeting oncogene ITGB1. *Oncotarget*. 2017;8(29):47389–47399.
49. Li L, Mao D, Li C, Li M. miR-145-5p Inhibits Vascular Smooth Muscle Cells (VSMCs) Proliferation and Migration by Dysregulating the Transforming Growth Factor-β Signaling Cascade. *Medical Science Monitor : International Medical Journal of Experimental and Clinical Research*. 2018;24:4894–4904.
50. Xiao Y, Peng H, Hong C, Chen Z, Deng X, Wang A, Yang F, Yang L, Chen C, Qin X. PDGF Promotes the Warburg Effect in Pulmonary Arterial Smooth Muscle Cells via Activation of the PI3K/AKT/mTOR/HIF-1α Signaling Pathway. *Cellular Physiology and Biochemistry*. 2017;42(4):1603–1613.
51. Dai Y, Duan H, Duan C, Zhu H, Zhou R, Pei H, Shen L. TCF21 functions as a tumor suppressor in colorectal cancer through inactivation of PI3K/AKT signaling. *OncoTargets and Therapy*. 2017;10:1603–1611.
52. Kim Y, Saville L, O'Neill K, Garant J-M, Liu Y, Haile-Merhu S, Ghashghaei M, Hoang QA, Louwagie A, Park YP, Jones SJM, Vu LP. Nanopore direct RNA sequencing of human transcriptomes reveals the complexity of mRNA modifications and crosstalk between regulatory features. *Cell Genomics*. 2025;5(6):100872.
53. Boo SH, Kim YK. The emerging role of RNA modifications in the regulation of mRNA stability. *Experimental & Molecular Medicine*. 2020;52(3):400–408.
54. Lockhart J, Canfield J, Mong EF, VanWye J, Totary-Jain H. Nucleotide Modification Alters MicroRNA-Dependent Silencing of MicroRNA Switches. *Molecular Therapy. Nucleic Acids*. 2019;14:339–350.
55. Letonja J, Petrovič D. A Review of MicroRNAs and lncRNAs in Atherosclerosis as Well as Some Major Inflammatory Conditions Affecting Atherosclerosis. *Biomedicines*. 2024;12(6):1322.
56. Lu Y, Thavarajah T, Gu W, Cai J, Xu Q. Impact of miRNA in Atherosclerosis. *Arteriosclerosis, Thrombosis, and Vascular Biology*. 2018;38(9):e159–e170.
57. Pardo-Palacios FJ, Wang D, Reese F, Diekhans M, Carbonell-Sala S, Williams B, Loveland JE, De María M, Adams MS, Balderrama-Gutierrez G, Behera AK, Gonzalez Martinez JM, Hunt T, Lagarde J, Liang CE, et al. Systematic assessment of long-read RNA-seq methods for transcript identification and quantification. *Nature Methods*. 2024;21(7):1349–1363.
58. Cappannini A, Ray A, Purta E, Mukherjee S, Boccaletto P, Moafinejad SN, Lechner A, Barchet C, Klaholz BP, Stefaniak F, Bujnicki JM. MODOMICS: a database of RNA modifications and related information. 2023 update. *Nucleic Acids Research*. 2024;52(D1):D239–D244.